534150

Sandia National Laboratories
Carlsbad Programs Group

Waste Isolation Pilot Plant

Effect of Naturally Occurring Sulfate on the MgO Safety Factor in the Presence of Supercompacted Waste and Heterogeneous Waste Emplacement

Author:	Joseph F. Kanney	(6821)		March 5 2004
	Print		Signature	Date
Author:	Anna C. Snider	(6822)		March 5, 2004
	Print		Signature	Date
Author:	T. William Thompson	(WRES)		March 5, 2004
	Print		Signature	Date
Author:	Laurence H. Brush	(6822)		March 5, 2004
	Print		Signature	Date
Technical Review:	Clifford W. Hansen	(6821)		March 5, 2004
	Print		Signature	Date
QA Review:	Mario J. Chavez	(6820)		March 5, 2004
	Print		Signature	Date
Management Review:	David S. Kessel	(6821)		March 5, 2004
	Print		Signature	Date

This page is left blank.

EXECUTIVE SUMMARY

Sandia National Laboratories (SNL) has performed a performance assessment (the AMW PA) to determine the effects of supercompacted waste and heterogeneous waste emplacement on repository performance at the Waste Isolation Pilot Plant (WIPP). Results of the AMW PA were submitted to the Environmental Protection Agency (EPA) by the Department of Energy (DOE) in order to obtain regulatory approval for disposal at WIPP of supercompacted INEEL waste (Hansen et al. 2004). EPA requested additional information regarding the effect of naturally occurring sulfate on the magnesium oxide (MgO) safety factor to complete their review (Marcinowski 2004). Sulfate reduction is one of the pathways for biodegradation of cellulosic, plastic and rubber materials (CPR) in the waste. Naturally occurring sulfate could increase the percentage of the CPR biodegraded by sulfate reduction, thereby decreasing in the MgO safety factor. EPA has requested an analysis on the amount of naturally occurring sulfate in the vicinity of the waste disposal area and a calculation of the impact that this additional sulfate could have on the MgO safety factor. EPA has requested that this analysis include several specific waste emplacement scenarios, including one that assumes a 50/50 volume split between supercompacted and uncompacted waste streams in a single panel.

Carbon dioxide (CO_2) produced by microbial degradation of CPR in the waste could adversely affect chemical conditions in the repository (lowering the pH and therefore increasing actinide solubilities). Magnesium oxide is emplaced in the repository to sequester CO_2, thus maintaining low CO_2 fugacity (f_{CO2}) and high pH conditions. The MgO safety factor is defined as the quantity of MgO available (the quantity emplaced in the repository or a panel adjusted to account for dissolution of MgO in brines and extent of MgO hydration) divided by the quantity of MgO required to consume the CO_2 that could be produced by biodegradation of the CPR. The conceptual model for WIPP geochemistry postulates that CPR biodegradation would be controlled by the sequential utilization of electron acceptors, resulting in the sequential degradation of CPR by denitrification, sulfate reduction and methanogenesis pathways. Denitrification and sulfate reduction produce 1 mole of CO_2 per mole of carbon consumed while methanogenesis produces 0.5 moles of CO_2 per mole of carbon consumed. Thus, the MgO safety factor will depend upon the amount of CPR and the fraction of CPR consumed by each of the three biodegradation processes. The fraction of CPR consumed by each of the processes will depend upon the amounts of nitrate and sulfate available in the system. Nitrate occurs only in the waste and reliable estimates of waste-derived nitrate are readily available. WIPP waste contains sulfate and natural sources of sulfate exist in the environment surrounding the repository.

This analysis provides a very conservative estimate of the impact that naturally occurring sulfate may have on the MgO safety factor. The approach used consists of the following steps: 1) identify natural sources of sulfate that may affect repository conditions and quantify the concentrations of sulfate in these sources; 2) identify and quantify sulfate transport processes which may bring sulfate into contact with the waste; 3) calculate the total amount of sulfate available to participate in microbial sulfate reduction for each loading scenario by

adding natural sulfate and waste-derived sulfate; 4) calculate the percentage of CPR degraded by denitrification, sulfate reduction and methanogenesis pathways for each loading scenario; and 5) calculate the resulting MgO safety factor based upon the ratio of CPR degraded by denitrification, sulfate reduction and methanogenesis. Finally, uncertainties involved in the analysis, and their impact on the analysis results, are discussed.

Sulfate occurs naturally in brines that are present in the Salado and Castile Formations, and in the minerals comprising the Salado. Processes that can result in mass transfer of sulfate into the repository include advection in brines, dissolution from sulfate-bearing minerals in surrounding rock, and diffusion through porous rock into the repository. Each of these processes is analyzed separately and their potential impacts are summed to arrive at an estimate of the total amount of naturally occurring sulfate. Thus, this analysis provides an estimate of the amount of naturally occurring sulfate that could be available to participate in the CPR biodegradation, based on the combined effect of many conservative assumptions that are incorporated into the analysis. These conservatisms include:

- Conservative estimates sulfate of concentration in WIPP brines are used in the calculations.
- Conservative estimates for the amount of sulfate-bearing minerals in rocks surrounding the repository are incorporated into the analysis.
- A conservative estimate for the CPR biodegradation time scale is incorporated into estimates for advective and diffusive sulfate transport.
- The estimates of advective sulfate flux are based on the maximum observed brine flow over all PA realizations, although the maximum flow has a very low probability of occurrence.
- The diffusion model assumes that the rock surrounding the repository is fully saturated with brine, although partially saturated conditions will exist for considerable periods of time. Diffusion rates in partially saturated porous media are considerably less than in saturated media.
- The estimates of sulfate diffusion incorporate a very conservative estimate for the porosity of the surrounding rock.
- Diffusive mass transfer limitations on the dissolution of sulfate-bearing minerals are completely neglected.

This analysis considers one homogeneous panel loading scenario and three emplacement scenarios in which a panel is preferentially loaded with supercompacted waste. The SNL homogeneous panel scenario assumes random waste emplacement, where supercompacted waste fills 11% of the panel's volume. The SNL realistic panel scenario assumes that supercompacted waste accounts for approximately 14% of waste volume in the panel. The SNL conservative panel scenario assumes that supercompacted waste accounts for approximately 27% of the waste volume in the panel. The EPA conservative panel scenario assumes 50/50 volume split between supercompacted waste and waste streams from sites other than INEEL. Considering that many sites will be shipping waste concurrently, and reflecting on the experience with shipments from the Rocky Flats Environmental Technology Site that went into Panel 1 (Leigh 2003), it is very unlikely that 50% of a panel will be filled with supercompacted waste.

Accounting conservatively for transport of naturally occurring sulfate into the panel decreases the calculated MgO safety factor relative to previous analyses that considered only sulfate in the waste (Snider 2003a, Hansen and Snider 2004). The MgO safety factor for the SNL homogeneous panel is 1.37, compared to 2.45 for previous estimates for the homogeneous 10-panel repository. For the SNL realistic and conservative cases, the safety factor decreases from 2.66 to 1.40 and from 2.02 to 1.13, respectively, when naturally occurring sulfate is included in the calculations. For the EPA conservative scenario, the safety factor is 0.94. Thus, even under the extremely conservative assumptions of this analysis, the MgO safety factor calculated on a panel basis is larger than 1.0 in all but the EPA conservative case. There is more than a reasonable expectation that more realistic modeling (see the list of conservative assumptions above) would result in a considerable increase in these calculated safety factors.

The results of this analysis show that the MgO safety factor is a function of both the sulfate available and the emplacement scenario. The MgO safety factor is shown to be more sensitive to the emplacement scenario (i.e., to the amount of CPR present) than to the amount of sulfate present. This analysis also indicates that dissolution and diffusion of sulfate into the waste panel is the main source of naturally occurring sulfate, although this may be largely a function of the conservatism used in the modeling.

The uncertainty analysis presented in this report addresses the sensitivity of the MgO safety factor to uncertainty in brine inflow volume, biodegradation time scale and effective diffusion coefficient. Results show that the MgO safety factor is only moderately sensitive to these variables and that the sensitivity decreases as more CPR is added to a panel.

TABLE OF CONTENTS

LIST OF TABLES

LIST OF FIGURES

1 Introduction

Sandia National Laboratories (SNL) performed an impact assessment to determine the effects of supercompacted waste and heterogeneous waste emplacement on repository performance at the Waste Isolation Pilot Plant (WIPP) (Hansen et al. 2004). The impact assessment addressed the emplacement of supercompacted waste processed by the Idaho National Engineering and Environmental Laboratory's (INEEL) Advanced Mixed Waste Treatment Project (AMWTP). The impact assessment took the form of a performance assessment, and is referred to as the AMW performance assessment (AMW PA). The results of the AMW PA were submitted to the Environmental Protection Agency (EPA) by the Department of Energy (DOE) in order to obtain regulatory approval for disposal at WIPP of supercompacted INEEL waste. EPA requested additional information regarding the effect of naturally occurring sulfate on the magnesium oxide (MgO) safety factor to complete their review (Marcinowski 2004). Sulfate reduction is one of the pathways for biodegradation of cellulosic, plastic and rubber materials (CPR) in the waste. Naturally occurring sulfate could increase the percentage of the CPR biodegraded by sulfate reduction, thereby decreasing the MgO safety factor. EPA has requested an estimate of the amount of naturally occurring sulfate that might be available to participate in microbial sulfate reduction and an analysis of the impact that this sulfate may have on the MgO safety factor. EPA has requested that this analysis include several waste emplacement scenarios, including one that assumes a 50/50 volume split between supercompacted and uncompacted waste streams in a single panel.

1.1 Objective

The objectives of this analysis are to: 1) provide a conservative estimate of the amount of naturally occurring sulfate that could be available to participate in the CPR biodegradation process; 2) quantify the impact of this sulfate might have on the MgO safety factor for a single panel for several emplacement scenarios involving supercompacted waste; and 3) identify and analyze sources of uncertainty.

1.2 Analysis Overview

This analysis provides a very conservative of the impact that naturally occurring sulfate may have on the MgO safety factor. The approach used consists of the following steps: 1) identify natural sources of sulfate that may affect repository conditions and quantifying the concentrations of sulfate in these sources; 2) identify and quantify sulfate transport processes which may bring sulfate into contact with the waste; 3) estimate the amount of waste-derived sulfate based upon different loading scenarios; 4) calculate the total amount of sulfate available to participate in microbial sulfate reduction for each loading scenario by adding natural sulfate and waste-derived sulfate; 5) calculate the percentage of CPR degraded by denitrification, sulfate reduction and methanogenesis pathways for each loading scenario; and 6) calculate the MgO safety factor based upon the ratio of CPR degraded by

denitrification, sulfate reduction and methanogenesis. Finally, uncertainties involved in this analysis are considered and estimates of their impact on the results obtained are discussed.

1.3 Report Outline

Section 2 presents the modeling approach used in this analysis. Section 3 presents results of the analysis. Section 4 discusses uncertainties involved in this analysis and estimates their impact on the results obtained. Finally, Section 5 summarizes the findings and presents conclusions.

2 Background and Approach

This section presents the approach used in this analysis. The CPR biodegradation process is reviewed. The role of sulfate and its impact on the MgO safety factor is discussed. The procedure for calculating MgO safety factor is reviewed. Sources of naturally occurring sulfate (SO_4^{2-}) are identified and the approach used to quantify and bound them is discussed. Processes which may transport sulfate into the repository are discussed, along with the methods used to quantify and bound their effects. The waste emplacement scenarios addressed in this analysis are described.

2.1 MgO Safety Factor and CPR Biodegradation

Carbon dioxide (CO_2) produced by microbial consumption of CPR in the waste could adversely affect chemical conditions in the repository (lowering the pH and therefore increasing actinide solubilities). Magnesium oxide (MgO) is emplaced in the repository along with the waste in order to sequester CO_2, thus maintaining low CO_2 fugacity (f_{CO2}) and high pH conditions. The MgO safety factor is defined as the quantity of MgO available (the quantity emplaced in the repository or a panel adjusted to account for dissolution of MgO in brines and extent of MgO hydration) divided by the quantity of MgO required to consume the CO_2 that could be produced by biodegradation of the CPR.

The conceptual model for WIPP geochemistry postulates that CPR biodegradation would be controlled by the sequential utilization of electron acceptors, resulting in the sequential degradation of CPR by denitrification, sulfate reduction and methanogenesis pathways (Brush 1990, Wang and Brush 1996, Francis et al. 1997):

$$C_6H_{10}O_5 + 4.8H^+ + 4.8NO_3^- \rightarrow 7.4H_2O + 6CO_2 + 2.4N_2 \quad (2.1)$$

$$C_6H_{10}O_5 + 6H^+ + 3SO_4^{2-} \rightarrow 5H_2O + 6CO_2 + 3H_2S \quad (2.2)$$

$$C_6H_{10}O_5 + H_2O \rightarrow 3CH_4 + 3CO_2 \quad (2.3)$$

While nitrate (NO_3^-) is available, CPR biodegradation will proceed by the denitrification pathway (Eq. 2.1) yielding 1 mole of CO_2 per mole of organic carbon (C) consumed. The only significant source of nitrate in the repository system is the WIPP waste. When nitrate in the waste has been exhausted, CPR consumption will proceed by the sulfate reduction pathway (Eq. 2.2) also producing 1 mole of CO_2 per mole of organic C consumed. WIPP waste contains some sulfate and naturally occurring sulfate in WIPP brines and Salado Formation minerals may also be available for microbial sulfate reduction. After the available sulfate has been utilized, CPR consumption will switch to methanogenesis (Eq. 2.3) which yields 0.5 moles of CO_2 per mole of organic C consumed. Thus, the MgO safety factor will depend upon the amount of CPR and the fraction of CPR consumed by each of the three biodegradation processes. The fraction of CPR consumed by each of the processes, in turn, will depend upon the amounts of nitrate and sulfate available in the system.

Sources of naturally occurring sulfate and transport processes that may bring sulfate into contact with the waste are addressed in Sections 2.2 and 2.3. The amount of CPR, nitrate and sulfate present in WIPP wastes is discussed in Section 2.4.

2.2 Sources of Naturally Occurring Sulfate

Sulfate occurs naturally in brines present in the Salado Formation and Castile Formation, and in the minerals comprising the Salado.

2.2.1 Salado and Castile Formation Brines

Geochemical analysis of interstitial brines in the Salado Formation surrounding the repository shows that they contain sulfate (Deal et al. 1995). Salado brines are relevant to this analysis because the Salado is in direct contact with the repository and there exist multiple pathways for sulfate in Salado brines to reach waste panels.

The Castile Formation, which underlies the Salado, contains isolated pressurized brine reservoirs (Swift and Corbet 2000). Geochemical analysis of Castile brine from the WIPP-12 and ERDA-6 boreholes indicate that these brines also contain sulfate (Popielak et al. 1983). Brine reservoirs in the Castile are relevant to this analysis because conceptual models for disturbed performance of the repository include a drilling intrusion that encounters one of these brine pockets (an E1 event), resulting in brine flow into the repository (U.S. DOE 1996, Section 6.3.2.2.2).

The two fluids that best represent the compositions of WIPP brines are: 1) Generic Weep Brine (GWB), which simulates intergranular (grain-boundary) fluids from the Salado Formation at or near the stratigraphic horizon of the repository; and 2) ERDA-6, typical of solutions in brine reservoirs in the underlying Castile (Brush and Xiong 2003b).

Snider (2003b) and Popielak et al. (1983) gave the concentrations of GWB and ERDA-6 prior to reaction with MgO. However, use of the sulfate concentrations predicted after reaction with MgO and waste constituents is more appropriate because it is consistent with the conceptual models of chemistry currently implemented in WIPP PA. Actinide solubility calculations assume that brines are at equilibrium with room contents (U.S. DOE 1996, Section 6.4.3.5). In addition, different MgO carbonation reactions buffer f_{CO_2} in the repository, depending on whether significant microbial gas production occurs (Brush and Xiong 2003a). These considerations result in six possible model brines, as shown in Table 1. This analysis uses the largest sulfate concentration predicted by these brine models.

Table 1. Models for Salado and Castile Brines

Salado Brine Models	Castile Brine Models
GWB Before Reaction	ERDA-6 Before Reaction
GWB After Reaction, Nonmicrobial	ERDA-6 After Reaction, Nonmicrobial
GWB After Reaction, Microbial	ERDA-6 After Reaction, Microbial

Once the brine sulfate concentration has been determined, the sulfate mass in a given volume of brine is calculated by

$$M_b^{SO_4} = C_b^{SO_4} V_b \tag{2.4}$$

where $M_b^{SO_4}$ is the mass of sulfate (kg), $C_b^{SO_4}$ is the sulfate concentration (kg m^{-3}), and V_b is the brine volume (m^3).

2.2.2 Salado Formation Minerals

Sulfate-bearing minerals such as anhydrite, gypsum and polyhalite exist in the Salado rock surrounding the disposal rooms (U.S. DOE 1983b, a). The chemical formulas for the main sulfate-bearing Salado minerals and their sulfate content are shown in Table 2. These minerals exist mainly in decimeter to meter scale "marker beds", and in thinner interbeds along with clays. They are also present as inclusions in the impure halites of the Salado (Swift and Corbet 2000). Figure 1 shows the Salado stratigraphy at the repository horizon. The waste disposal region is excavated within an approximately 7 m-thick section between anhydrite marker beds 138 (MB 138) and 139 (MB 139). MB 138 is approximately 0.85 m thick while MB 138 is approximately 0.18 m thick. Two thinner anhydrite interbeds, known as anhydrites a and b, occur between the repository and MB 138 (Swift and Corbet 2000).

Table 2. Major Sulfate-bearing Minerals in the Salado

Mineral	Formula	Mass Fraction SO_4^{2-}
Anhydrite	$CaSO_4$	0.706
Gypsum	$CaSO_4 \cdot 2H_2O$	0.558
Polyhalite	$K_2MgCa_2(SO_4)_4 \cdot 2H_2O$	0.637

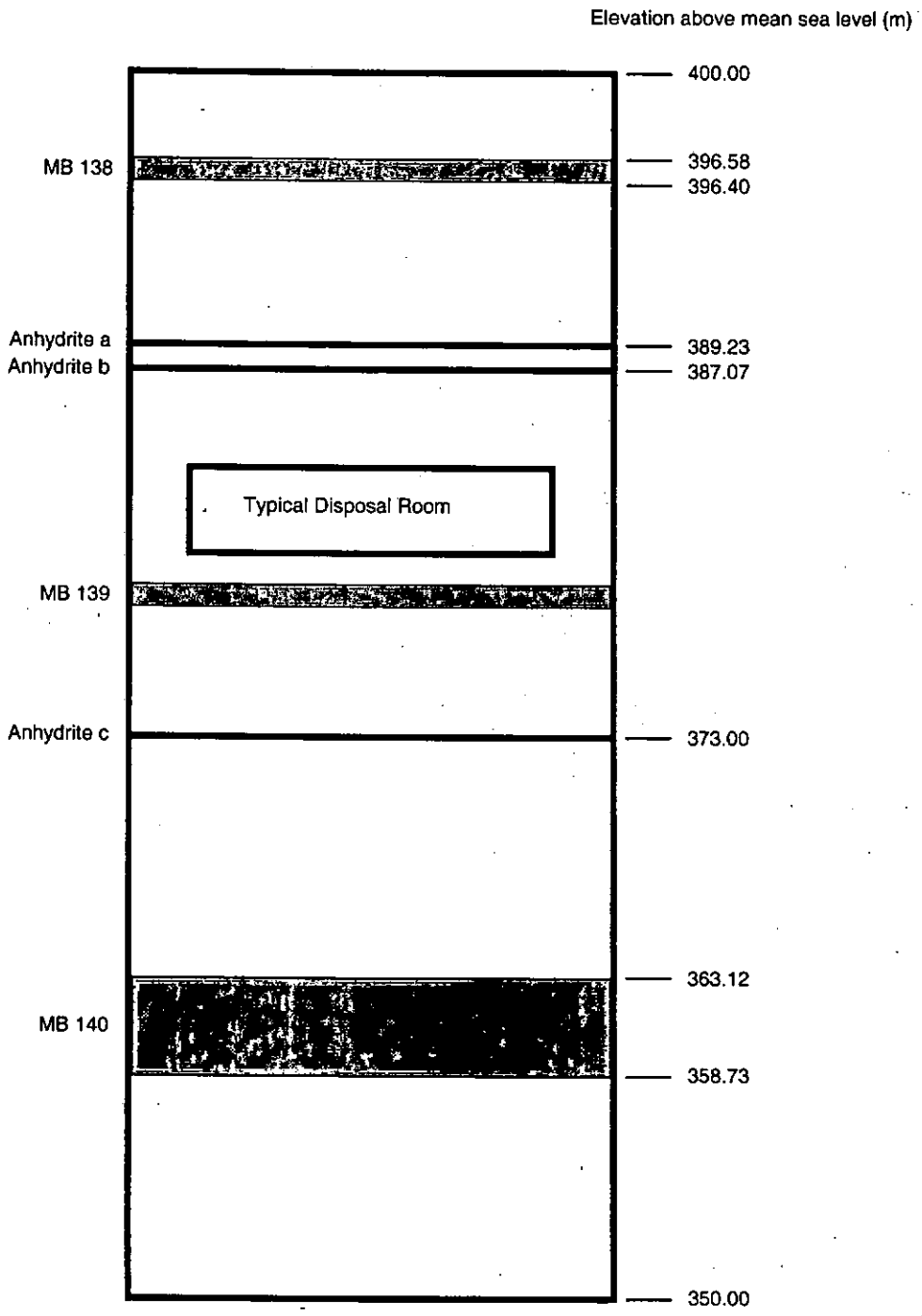

Figure 1 Salado Stratigraphy at the Horizon of the WIPP (WIPP PA 1992)

Stein (1985) analyzed 46 samples from two 50-ft-long, 4.5-in-diameter cores drilled vertically up through the back, and vertically down through the floor of Test Room 4 in the northern (experimental) end of the WIPP underground workings. These cores were drilled for the Site and Preliminary Design Validation (U.S. DOE 1983b, a). Brush (1990) used Stein's results to establish a composition of 93.2 wt % halite (NaCl) and 1.7 wt % each of the minerals anhydrite, gypsum, magnesite ($MgCO_3$), and polyhalite. This composition is the average mineralogical composition of the stratigraphic intervals sampled by these 2 50-ft cores because Stein's samples included all of the lithologies present in these intervals (nearly pure halite, argillaceous halite, polyhalitic halite, mixed argillaceous-polyhalitic halite, and anhydrite-and-clay seams). Stein quantified the concentrations of halite in these cores by weight loss upon dissolution of this mineral by distilled water; the average concentration of halite was 93.2 wt %. The concentrations of anhydrite, gypsum, magnesite, polyhalite, and silicate minerals (mainly clays) could not be quantified by the X-ray-diffraction technique used by Stein. Therefore, Brush assumed equal concentrations of anhydrite, gypsum, magnesite, and polyhalite, which he assumed constitute a total of 6.8 wt % of the Salado (the portion consisting of minerals other than halite). Brush omitted bassanite ($CaSO_4 \cdot 0.5H_2O$) because it only appeared in the diffractogram for one of Stein's samples. Furthermore, Brush omitted silicates because geochemical speciation-and-solubility codes cannot model the behavior of Al- and Si-bearing aqueous species in high-ionic-strength brines. (There are insufficient Pitzer ion-interaction parameters for Al and Si.) Omission of clays, which are probably present at about the same concentration as each of the evaporite minerals (anhydrite, gypsum, magnesite, and polyhalite), increased the concentrations of these four evaporite minerals somewhat because they were assumed to constitute the entire nonhalite fraction of the rock. Additional details are provided in U.S. DOE (1983b), Stein (1985), and Brush (1990).

Given an average mineralogical composition for the Salado, one can compute a sulfate density from

$$\rho_r^{SO_4} = \rho_{halite} \sum_{i=1}^{N_m} \chi_{Salado}^{i} \chi_i^{SO_4} \tag{2.5}$$

where $\rho_r^{SO_4}$ is the sulfate density in Salado rocks (kg m^{-3}), ρ_{halite} is the density of halite (kg m^{-3}), N_m is the number of sulfate-bearing minerals, χ_{Salado}^{i} is the mass fraction of the *ith* mineral in Salado rock (dimensionless), and $\chi_i^{SO_4}$ is the mass fraction of sulfate in the *ith* mineral (dimensionless).

2.3 Sulfate Transport Processes and Pathways

Naturally occurring sulfate must be transported into the waste rooms in order to participate in CPR biodegradation. Processes which can result in mass transfer of sulfate into the repository include advection, dissolution, and diffusion. Advection is the transport of solute by bulk movement of a fluid. The fluid in this case will be brines flowing into the waste panel. Diffusion is the transport of solutes across a concentration gradient by molecular

motion. When fluid velocities are low, diffusion can be a significant solute transport mechanism. Dissolution is the interphase mass transfer of a solute from the mineral solid phase to the fluid phase. Dissolution will occur when the fluid phase solute concentration falls below a characteristic saturation value, which is a function of the mineral and fluid composition. Although advection, diffusion, and dissolution are, in general, coupled processes, this analysis will consider and provide a conservative bound on each process separately.

2.3.1 Time Scale

To estimate the amounts of sulfate that may be transported into the repository, one must select an appropriate time scale. In this case, the appropriate time scale is the period during which CPR biodegradation will occur. In this analysis, we will refer to the time scale for CPR biodegradation as T_{bio}. The biodegradation time scale will vary with the brine saturation conditions in the repository since the biodegradation rate is a function of brine saturation. Brine saturations and biodegradation of CPR as a function of time can be obtained from the output of BRAGFLO simulations.

Since variable saturation conditions within the repository will result in variable rates of CPR biodegradation, the most appropriate approach to evaluate T_{bio} is to examine the BRAGFLO output variable for CPR remaining in the repository (CELL_REM). An estimate for T_{bio} can be obtained by observing the time at which CELL_REM goes to zero, or attains some constant value. This method is appropriate since it takes into account uncertainties in brine saturation within the repository.

2.3.2 Advection

Sulfate could be advected into the repository in Salado and Castile brines, so a bounding estimate on sulfate available for sulfate reduction needs to address advection pathways and magnitudes. Since the pathways will differ under disturbed and undisturbed conditions, they are discussed separately.

2.3.2.1 Undisturbed Conditions

Under undisturbed conditions, Salado brines can only come into contact with the waste by flowing from the disturbed rock zone (DRZ) into the repository. The only significant external source of brine to the DRZ is from the anhydrite marker beds (Helton et al. 1998). The extent of the DRZ, and its development in time, has been estimated using the relationship between mean and deviatoric stresses calculated for various scenarios. Further information is given in Hansen (2003).

In evaluating the likelihood of fractures forming significant advective pathways under undisturbed conditions, two different sets of conditions must be considered: 1) those in which

gas pressures are less than lithostatic; and 2) those in which gas pressures reach and exceed lithostatic. Additionally, we need to consider the situations both in Panels 1 and 2, where the disposal rooms are at the original repository horizon and in the later panels where the rooms will be raised so that the back coincides with Clay Seam G.

2.3.2.1.1 Gas Pressures Less Than Lithostatic

In the case of gas pressures less than lithostatic, healing of the salt back and floor may be expected to isolate the surrounding sulfate bearing strata from advective flow.

Hansen (2003) has used calculated stress distributions around a disposal room, and their development with time, to examine the growth and healing of the salt DRZ. These calculations depend on a relationship between the mean compressive stress (I_1) and the second invariant of deviatoric stress (J_2) developed from lab data to define the stress envelope separating undilated salt from the dilated salt characteristic of the DRZ. This relationship describes a set of conditions such that when the deviatoric stresses are high relative to the mean normal stresses the DRZ develops, and when the mean normal stresses dominate the DRZ heals. The results of these calculations are summarized in Figure 2 (from Hansen, 2003), and show that the salt DRZ develops immediately on excavation, and grows somewhat in time until the closure of the room causes the back to contact the waste. After this, the waste exerts an ever increasing back pressure on the roof and floor, causing the DRZ above and below the room to heal and reduce in extent. The healing of salt has been demonstrated by Costin and Wawersik (1980), who conducted a number of laboratory experiments on salt healing. They showed that samples which had been fractured by tensile stresses healed rapidly (in a week or less) under minimal compressive stresses.

The calculations included in Hansen (2003), and summarized in Figure 2, show that after only 50 years the DRZ has reduced in size sufficiently to heal any potential pathways to MB 139, for the case of the room being mined up to Clay G. Hansen noted that "In fewer than 100 years the state of stress in the salt around the waste rooms will approach equilibrium, and the DRZ around the greater areas of the waste rooms would be largely healed as well". Since creep closure and back pressure from the waste increase the compressive stresses in the back in both the vertical and horizontal directions, any pathways due to bolting may also be expected to be closed in a similar time period. The healing of the salt DRZ, under even small back pressures, will therefore isolate the disposal room from the over and underlying rocks from any but diffusive transport mechanisms. It is likely that the relatively brittle anhydrites will continue to sustain fractures; however the healing of the salt strata between these anhydrites and the disposal rooms will effectively isolate them.

The situation will be a little different laterally, since closure of the ribs against the waste is expected to take significantly longer than the vertical closure, and therefore the DRZ in the ribs may be expected to last longer as well. Advective access to sulfate bearing rocks, including Anhydrite B, in the ribs will last longer. It should be noted that the likely maximum extent of the lateral DRZ is of the order of a maximum of 3 m (Hansen 2003). Also, over much of this region, fracturing will be parallel to the wall and will therefore not provide access for brine.

In the case of Panel 1, which was open for more than 15 years, fracturing is quite extensive, particularly in the floor where heave opened sizeable fractures down to marker bed (MB) 139. In this panel the floor heave has been severe enough that the floor had to be remined on several occasions, such that the distance of the room from the marker bed was reduced by about 1 m. Floor heave of this severity has not been observed in Panel 2, which has only been open for about 4 years. Panel 3, and subsequent panels, are to be mined at a horizon 2.43 m higher than Panels 1 and 2, with the back at Clay G. This change means that the separation from MB 139 is increased to 3.8 m so that floor heave is highly unlikely, and fracture connections to MB 139 are not anticipated. In the back, Anhydrite B (above Clay G) is removed to ensure good roof conditions.

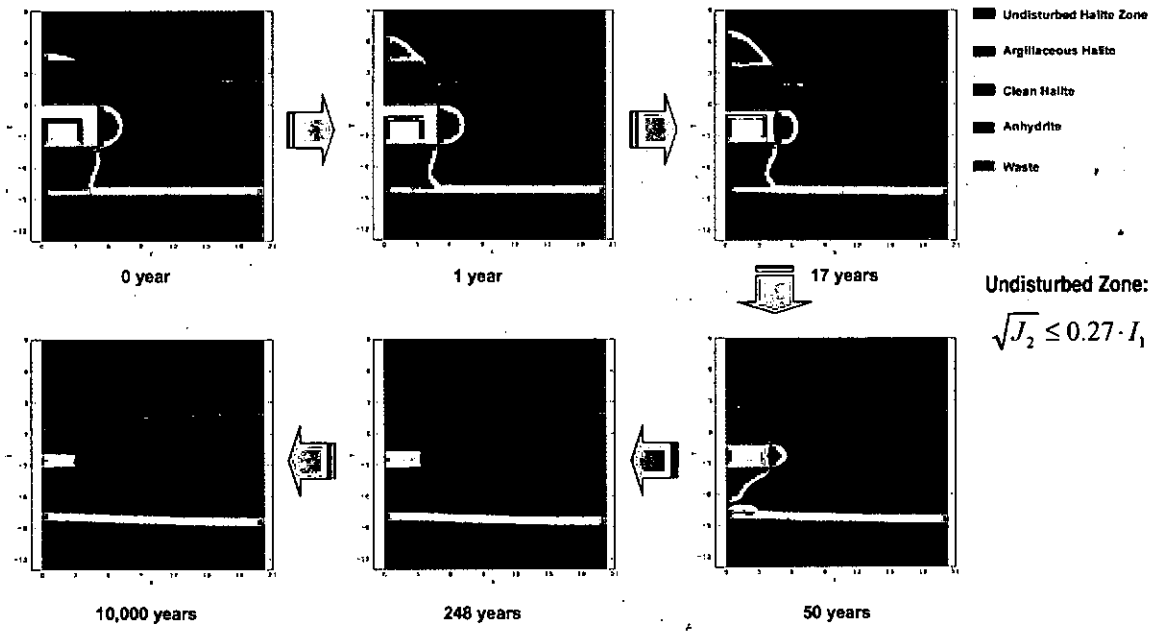

Figure 2. Disturbed Rock Zone around a Raised Disposal Room with Time for f=0.0

2.3.2.1.2 Gas Pressure Greater Than Lithostatic

Under certain conditions gas pressures may exceed the lithostatic stress, and under these conditions fracturing of the surrounding rocks will occur, the fractures extending to the point where the increase in pore volume is sufficient to reduce the pressure back to lithostatic. However, the gas-induced fracture model of the BRAGFLO code should capture the effects that this type of fracturing of the DRZ and anhydrite layers may have on brine flows.

The assumption has been made for those panels at the original horizon, and where the Option D panel closure is used, that gas-induced fracturing will be through MB 139, by-passing the closure. In the panels at the higher horizon (Clay G) this by-pass is likely to be either through the salt, or potentially along the parting associated with Clay G and Anhydrite B or Clay H and Anhydrite A. Although at first sight it appears that these fractures might provide

a pathway for advective flow from the surrounding strata, this access will be for a limited duration. During fracture propagation, and as long as the pressure is maintained sufficiently for these fractures to be open, the gas pressure in the fracture will be higher than the far-field pressures in the interstitial brines. This pressure differential may be expected to prevent brine flow out of the porous media adjacent to the fracture and from the far-field.

Pressures in the fracture could fall below lithostatic over time if there is leak-off of high pressure gas into the formation in excess of the rate of generation of additional gas. Under these conditions, the fractures will close under the effects of the rock stress: those fractures in halite will close, and potentially heal, to a very low permeability that will effectively seal the high-sulfate rocks from the disposal room. In this case, therefore, access to the sulfate-bearing rocks will be limited. In the case of Panels 1 and 2, there may be some access to MB 139. In the higher panels however, any contact will be to the thinner anhydrites (Anhydrite B and possibly Anhydrite A) and the flow of brine from these layers will be very limited by pressure and capillarity, and by fracture closure and healing after gas pressure drops.

With regard to the effects of gas-induced fracturing described above, it should be stressed that the BRAGFLO code used to model brine and gas flow in the vicinity of the repository implements a fluid flow model which is coupled to the rock system (WIPP PA 2003). The fracture treatment in BRAGFLO allows for pressure–induced alterations to the porosity in the DRZ and in the anhydrite interbeds. The BRAGFLO fracture treatment further allows for change in the fracture material permeability. Because of the conservative nature of the fracture model implemented, the brine flows predicted by BRAGFLO should be a reasonable bound for fracture flow in the repository system.

2.3.2.2 Disturbed Conditions

Conceptual models for disturbed performance of the repository include scenarios involving drilling intrusions. An E1 event refers to a single drilling intrusion through the repository that penetrates pressurized brine in the Castile Formation. An E2 event refers to a single drilling intrusion through the repository that does not encounter brine in the Castile (U.S. DOE 1996, Section 6.3.2.2.2) These events provide additional pathways for brine to enter the repository. In E1 intrusions, brine may flow down the intruding borehole from overlying formations, and brine may flow up the borehole form a pressurized pocket in the Castile. In E2 intrusions, brine may only flow downward from overlying formations. These types of intrusions are included in numerical simulations of brine and gas flow (using the BRAGFLO code) as shown in Table 3.

Table 3. BRAGFLO Modeling Scenarios

Scenario	Description
S1	Undisturbed repository
S2	E1 intrusion at 350 years
S3	E1 intrusion at 1000 years
S4	E2 intrusion at 350 years
S5	E2 intrusion at 1000 years
S6	E2 intrusion at 1000 years; E1 intrusion into same waste panel at 2000 years

BRAGFLO simulations performed to support the Compliance Certification Application (CCA) and the Compliance Recertification Application (CRA-2004) indicate that brine inflow volumes associated with drilling into a Castile brine pocket are typically over 200% greater than the inflow volumes encountered in the undisturbed case (Helton et al. 1998, Stein and Zelinski 2003). Thus, it is almost certain that intrusion scenarios will result in a larger estimate for the sulfate advection process.

2.3.2.3 Bounding Estimate for Advection

The preceding discussions regarding possible advective processes can be summarized as follows: 1) DRZ healing will tend to remove advective pathways not associated with drilling intrusions or gas-induced fracturing; 2) the effects of drilling intrusions and gas-induced fracturing are included in PA using BRAGFLO modeling; and 3) BRAGFLO simulations indicate that brine flows due to intrusions are much greater than during undisturbed conditions. Therefore, a very conservative bound on sulfate advection can be obtained by using the maximum brine flow predicted by the BRAGFLO code. It should be noted that we focus on the flow into a single panel from a single E1 event because of tight panel closures. The panel closures prevent substantial cross-flow of brine into other panels after an E1 intrusion.

A bound on the amount of brine flow into a panel by advection can be obtained by examining the BRAGFLO output variable for total brine flow into a waste panel (BRNWPIC). If we select the maximum value of BRNWPIC during the time interval $[0, T_{bio}]$, then a bound on the amount of sulfate advected into any given panel in the repository during a period of time consistent with the biodegradation time scale is given by

$$M_b^{SO_4} = V_b^{\max} C_b^{SO_4} \tag{2.6}$$

where $M_b^{SO_4}$ is the mass of sulfate advected in brines (kg), $V_b^{\max}$ is the maximum cumulative brine inflow (m^3), and $C_b^{SO_4}$ is the sulfate concentration in the brine (kg m^{-3}).

2.3.3 Diffusion and Dissolution

Even in the absence of significant brine flow, saturated or partially saturated conditions may exist in large portions of the DRZ for extended periods. In the absence of advection, the only significant mechanism for sulfate transport would be diffusion in DRZ pore waters. The driving force for sulfate diffusion would be a concentration gradient between the brine in waste rooms and brine in the DRZ pores. As sulfate reduction in waste rooms consumes sulfate, brine in the waste rooms will be depleted in sulfate (see Figure 3).

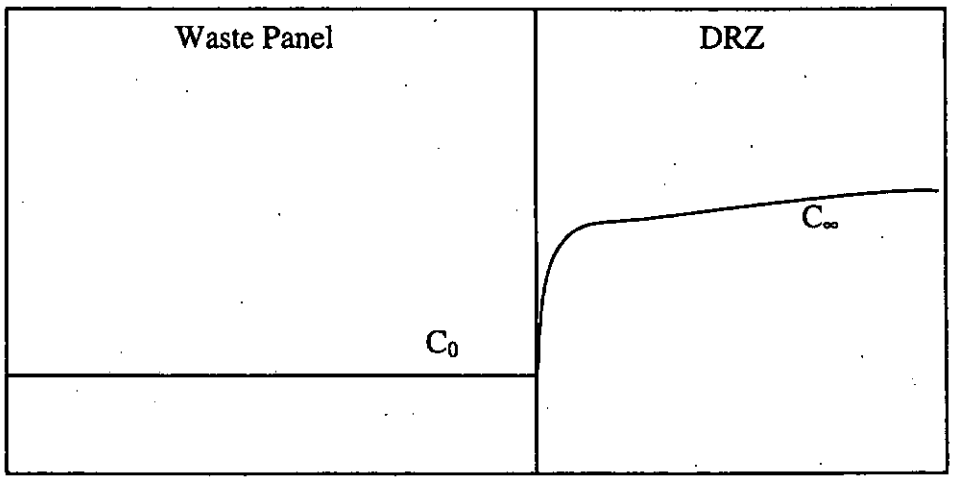

Figure 3. Sulfate Diffusion from DRZ into Waste Panel

If there is considerable diffusion of sulfate out of the DRZ pores into the repository, it is possible that sulfate concentrations in DRZ pore waters might be reduced to the point where sulfate would dissolve from the sulfate-bearing minerals within the DRZ. However, the sulfate dissolution process itself would be subject to diffusive mass transfer limitations since dissolution would occur mainly at grain boundaries. Significant mass-transfer limitations would be encountered in moving sulfate from intergrain spaces into the pore space. One should note that sulfate dissolution would not come into play when advection dominates because Salado and Castile brines will be in equilibrium with sulfate bearing minerals in the rock due to being in contact with them for millions of years.

An extremely conservative estimate of the amount of sulfate that may dissolve and diffuse into the repository can be obtained by ignoring any mass transfer limitations on sulfate dissolution and assuming that all mineral-associated sulfate within a given volume of rock will diffuse into the waste panel and will be available to participate in the sulfate reduction reaction. The appropriate volume of rock to consider is that volume which lies within a boundary defined by a diffusion length consistent with the time scale of interest:

$$V_r = L_{diff}^{SO_4} S_p \tag{2.7}$$

where $L_{diff}^{SO_4}$ is a characteristic diffusion length (m), and S_p is the surface area of the waste panel (m^2). The amount of sulfate in this volume can be calculated using

$$M_{diff}^{SO_4} = \rho_r^{SO_4} V_r \tag{2.8}$$

2.3.3.1 Characteristic Diffusion Length

The rate of diffusive mass transfer from the DRZ pore waters into a panel can be modeled using Fick's Law (Freeze and Cherry 1979).

$$F_{diff}^{SO_4} = -S\phi D_{eff}^{SO_4} \left[\frac{\partial C^{SO_4}}{\partial x} \right]_{x=0} \tag{2.9}$$

where $F_{diff}^{SO_4}$ is the rate of diffusive mass transfer (kg s^{-1}), S is the surface area of the waste panel (m^2), ϕ is the DRZ porosity (dimensionless), $D_{eff}^{SO_4}$ is the effective diffusion coefficient of sulfate in DRZ pore water ($m^2 s^{-1}$), $C^{SO_4}(x,t)$ is the sulfate concentration in DRZ pore water (kg m^{-3}), x is the distance into the DRZ along a direction normal to the panel wall, ceiling, or floor (m), and t is time (s).

The effective diffusion coefficient of a solute in a saturated porous medium such as the DRZ is given by

$$D_{eff}^{SO_4} = D_0^{SO_4} \phi \tau \tag{2.10}$$

where D_0 is the free liquid diffusion coefficient ($m^2 s^{-1}$), ϕ is the porosity (dimensionless), and τ is the porous media tortuosity (dimensionless) (de Marsily 1986).

The governing partial differential equation (PDE) for solute diffusion in a fluid saturated porous media a variation of the classic equation for of heat conduction developed by Fourier (Freeze and Cherry 1979)

$$\frac{\partial C^{SO_4}}{\partial t} = D_{eff}^{SO_4} \frac{\partial^2 C^{SO_4}}{\partial x^2} \tag{2.11}$$

Appropriate initial and boundary conditions for the situation sketched in Figure 2 are

$$C^{SO_4}(x,0) = C_\infty \quad \text{for } x \in [0, L_{DRZ}] \tag{2.12}$$

$$C^{SO_4}(0,t) = C_0 \quad \text{for } t > 0 \tag{2.13}$$

$$C^{SO_4}(L_{DRZ},t) = C_\infty \quad \text{for } t > 0 \tag{2.14}$$

For $x < L_{DRZ}$, the PDE problem described by Eqs. 2.11-2.14 admits the following analytical solution (Cussler 1997)

$$\frac{C^{SO_4} - C_0}{C_\infty - C_0} = \text{erf}\left(\frac{x}{\sqrt{4D_{eff}^{SO_4} t}}\right) \tag{2.15}$$

where

$$erf(z) = \frac{2}{\sqrt{\pi}} \int_0^z e^{-s^2} ds \tag{2.16}$$

is known as the error function (Abramowitz and Stegun 1972).

The nondimensional argument for the error function in Eq. 2.15 defines a characteristic diffusion length scale:

$$L_{diff}^{SO_4} = \sqrt{4D_{eff}^{SO_4} T_{bio}} \tag{2.17}$$

In physical terms, this is the length at which concentration attains 85% of the far-field value.

2.3.3.2 Bounding Estimate of Effective Diffusion Coefficient

For a given time, a conservative estimate for the diffusion length is obtained from a bounding estimate for effective diffusion coefficient. The effective diffusion coefficient, in turn, depends upon the free liquid diffusion coefficient, porosity, and tortuosity. The approach for estimating these quantities is described below.

The free liquid diffusivity of sulfate in WIPP brines can be effectively bounded by its value in sea water since the ionic strength of WIPP brines is approximately an order of magnitude larger than that of sea water. Geochemical modeling of WIPP brines using the FMT code was performed in support of actinide solubility calculations for the CRA (Brush and Xiong 2003a). FMT simulations used for the actinide solubility calculations show that the ionic strength of WIPP brines is approximately 6.7 m to 7.5 m (see FMT output files AP098_FMT_RUN12.OUT, AP098_FMT_RUN12.OUT, AP098_FMT_RUN22.OUT, and Ap098_Fmt_Run28.Out in CMS library LIB_AP098_FMT). The average ionic of average sea water is approximately 0.7 m (Stumm and Morgan 1996).

The initial porosity of the DRZ surrounding the waste panels is a sampled parameter in the WIPP PA (DRZ_1:POROSITY), but this initial DRZ porosity is allowed to increase in response to gas pressures in BRAGFLO modeling. Thus, a bounding estimate for ϕ can be obtained by using the maximum value of the DRZ porosity allowed in the BRAGFLO calculations.

There are no direct measurements of DRZ tortuosity, but it may be estimated using the formation factor from geophysics (de Marsily 1986):

$$\tau = \frac{1}{F\phi} \tag{2.18}$$

where the formation factor, F, is defined as the ratio of the electric resistivity of the rock to the resistivity of the contained water. F can be related to porosity by the Archie equation (Archie 1942):

$$F = \frac{1}{\phi^m} \tag{2.19}$$

where m is an empirical exponent, often referred to as the cementation factor. Substituting Eq. 2.19 into Eq. 2.18, we obtain a relationship between tortuosity and porosity:

$$\tau = \phi^{m-1} \tag{2.20}$$

The cementation factor must be determined experimentally. Electromagnetic induction logging to determine moisture content was performed for 28 boreholes in the Salado formation at the stratigraphic horizon of the WIPP facility in 1988 (Deal et al. 1989). Comparison of moisture contents determined by this technique with moisture contents determined by physical sample analysis revealed that an Archie equation exponent of $m = 1.8$ closely represented average conditions in the WIPP stratigraphy. This is the value used in this analysis.

2.4 Waste Emplacement Scenarios

Since the objective of the AMW PA was to evaluate the impact of heterogeneous waste emplacement that could result from the disposal of the supercompacted waste, models were developed for the WIPP repository with one panel (referred to as panel X) preferentially loaded with supercompacted waste and the remaining waste distributed homogeneously throughout the rest of the repository (Hansen et al. 2004). Since preferentially loading one panel with supercompacted waste will result in larger amounts of CPR in that panel, the MgO safety factor in that panel may be impacted.

This analysis will consider the effects of sulfate reduction for the scenario of a single panel with homogeneous waste emplacement and for several scenarios in which a panel is preferentially loaded with supercompacted waste. In order to preserve continuity with previous reports, the waste emplacement scenarios considered in this analysis are labeled as follows: 1) the SNL homogeneous panel X scenario; 2) the SNL realistic panel X scenario; 3) the SNL conservative panel X scenario; and 4) the EPA conservative panel X scenario. All scenarios except the SNL homogeneous panel X explicitly include the assumption that a

TDOP occupies a space in the WIPP repository equivalent to two seven-packs of 55-gallon drums. These emplacement scenarios are described briefly below.

The SNL homogeneous panel X scenario assumes random waste emplacement. The homogeneous waste mix incorporates all sites other than INEEL, all 55-gallon drums from INEEL, and all INEEL waste in standard waste boxes (SWBs), ten-drum overpacks (TDOPs), and 100-gallon drums of supercompacted waste. Supercompacted waste accounts for approximately 12% of the waste volume in this scenario (Hansen et al. 2004). The waste material properties for this scenario are calculated in Leigh (2004a).

The SNL realistic panel X scenario assumes that supercompacted waste accounts for approximately 14% of waste volume in the panel. A detailed description of the waste loading assumptions for this scenario was first presented in Leigh (2003). An updated discussion which includes the assumption that a TDOP occupies a space in the WIPP repository equivalent to two seven-packs of 55-gallon drums and presents the resulting waste material properties is contained in Leigh (2004b).

The SNL conservative panel X scenario assumes that supercompacted waste accounts for approximately 27% of the waste in the panel. A detailed description of the waste loading assumptions for this scenario is presented in Leigh (2003). An updated discussion which includes the assumption that a TDOP occupies a space in the WIPP repository equivalent to two seven-packs of 55-gallon drums and presents the resulting waste material properties is contained in Leigh (2004b).

The EPA has requested an analysis in which Panel X is be loaded with supercompacted waste and waste from sites other than INEEL without any of the AMWTF non-debris waste in the panel (Marcinowski 2004). In response, this analysis will consider such an emplacement scenario, referred to here as the EPA conservative panel X scenario. The EPA conservative panel X scenario assumes 50/50 volume split between supercompacted waste and waste from other waste streams (i.e., sites other than INEEL). The waste material parameters for this configuration are presented in Leigh (2004a).

Table 4 summarizes the mass of contact-handled CPR (CH CPR), nitrate, and sulfate in WIPP waste for the homogeneous panel X, SNL realistic panel X, SNL conservative panel X, and EPA conservative panel X emplacement scenarios. The sulfate in the last column of this table is added to the naturally occurring sulfate to arrive at the total amount of sulfate available to participate in the sulfate reduction reaction. One should note that the amount of CPR in the EPA conservative panel X is approximately 1.3 times larger than the SNL conservative panel X, approximately 2 times larger than SNL realistic panel X, and approximately 2.2 times larger than the SNL homogeneous panel X.

Table 4. Waste-derived CH CPR, Nitrate and Sulfate in Panel X

Scenario	CH CPR[1] (kg)	Nitrate (kg)	Sulfate (kg)
SNL Homogeneous [2]	3.00×10^6	2.62×10^5	4.40×10^4
SNL Realistic [3]	3.34×10^6	2.75×10^5	3.90×10^4
SNL Conservative [3]	4.89×10^6	2.69×10^5	1.40×10^4
EPA Conservative[2]	6.52×10^6	1.23×10^5	2.63×10^4

1. Cellulose equivalents (mass of cellulose + 1.7 *mass of plastics + mass of rubber)
2. (Leigh 2004a)
3. (Leigh 2004b)

Based on the calculated quantities of sulfate available for sulfate reduction, the MgO safety factors for the SNL homogeneous panel X, SNL realistic panel X, SNL conservative panel X, and EPA conservative panel X are calculated in Microsoft Excel workbooks following the methodology documented in Snider (2003a) and Hansen and Snider (2004). The workbooks for this analysis all include a worksheet entitled "Sulfate Contribution". This sheet displays calculations for the moles of sulfate present in maximum brine inflow and the moles of sulfate available by diffusion from the surrounding DRZ. In the worksheets entitled "CH CPR", a new column, labeled "waste+brine+DRZ", is added under the "moles of nitrate and sulfate initially present in the waste" portion of the sheet. The new column calculates the moles of total sulfate available for sulfate reduction by adding the moles of sulfate present in the waste plus the moles of sulfate in the brine plus the moles of sulfate available from the DRZ. The molar fraction of cellulosics biodegraded via sulfate reduction is changed accordingly to include the complete sulfate mole contribution. The new number changes the contribution of biodegradation from methanogenesis thus affecting the MgO safety factor. The equations for the percentage of CPR degraded by denitrification and sulfate reduction were modified to account for the boundary cases of excess nitrate and sulfate.

3 Results

This section presents the estimates of available sulfate and calculates the impact on the MgO safety factor. In anticipation of the uncertainly analysis, the results presented in this section will be referred to as the baseline case.

3.1 Sulfate Content of Brines and Minerals

The estimates for the sulfate content of WIPP brines Salado minerals are presented below.

3.1.1 Sulfate Content of Salado and Castile Brines

Table 5 provides the concentrations of GWB and ERDA-6 brines before and after reaction with the MgO engineered barrier. Note that reaction with MgO increases the sulfate concentrations slightly in three cases (GWB, nonmicrobial; GWB, microbial; and ERDA-6, nonmicrobial) and decreases its concentration slightly in one case (ERDA-6, microbial). In order to provide a bounding estimate of the naturally occurring sulfate in WIPP brines, we will use the largest sulfate brine concentration in Table 5 (182 mM or 17.483 kg m^{-3}).

Table 5. Compositions of GWB and ERDA-6 Before and After Reaction with MgO.

Element or Property	GWB, Before Reaction[1]	GWB, After Reaction, Non-microbial[2]	GWB, After Reaction, Microbial[3]	ERDA-6, Before Reaction[4]	ERDA-6, After Reaction, Non-microbial[5]	ERDA-6, After Reaction, Microbial[6]
SO_4^{2-}	175 mM	182 mM	182 mM	170 mM	176 mM	169 mM
$B(OH)_3$	155 mM	144 mM	144 mM	63 mM	23.4 mM	21.4 mM
Na^+	3.48 M	4.33 M	4.33 M	4.87 M	5.29 M	5.32 M
Mg^{2+}	1.00 M	582 mM	582 mM	19 mM	146 mM	147 mM
K^+	458 mM	487 mM	487 mM	97 mM	96.0 mM	96.1 mM
Ca^{2+}	14 mM	11.0 nM	11.0 mM	12 mM	11.8 mM	12.4 mM
Cl^-	5.51 M	5.43 M	5.43 M	4.8 M	5.24 M	5.25 M
Br^-	26 mM	27.7 mM	27.7 mM	11 mM	10.9 mM	10.9 mM
TIC	NR[7]	0.4 mM	0.4 mM	NR[7]	0.1 mM	0.5 mM
Log f_{CO_2}	NR[7]	-5.48	-5.50	NR[7]	-6.15	-5.50
pH	NR[7]	8.69	8.69	6.17	8.99	9.02

1. Snider (2003).
2. FMT Run AP098_FMT_Run012.OUT. (CMS library LIB_AP098_FMT).
3. FMT Run AP098_FMT_Run018.OUT. (CMS library LIB_AP098_FMT)
4. Popielak et al. (1983).
5. FMT Run AP098_FMT_Run022.OUT. (CMS library LIB_AP098_FMT)
6. FMT Run AP098_FMT_Run028.OUT. (CMS library LIB_AP098_FMT)
7. NR = not reported.

3.1.2 Sulfate Content of Salado Minerals

Using 1.7 wt % for the amount of each of the minerals anhydrite, gypsum and polyhalite in the Salado, the mass fractions of sulfate in each mineral from Table 2, the sulfate density of Salado rock can be calculated from Eq. 2.5. The results of this calculation are shown in Table 6.

Table 6. Sulfate Content of Salado Rock[1]

Mineral	Mass Fraction of Mineral in Salado χ^i_{Salado} (-)	Mass Fraction of Sulfate in Mineral $\chi_i^{SO_4}$ (-)	Sulfate Mass in Unit Volume of Salado Rock Due to Mineral $\rho_{halite}\chi^i_{Salado}\chi_i^{SO_4}$ (kg m^{-3})
Anhydrite	1.7×10^{-2}	0.706	25.910
Gypsum	1.7×10^{-2}	0.558	20.488
Polyhalite	1.7×10^{-2}	0.637	23.401
Sulfate Mass in Unit Volume of Salado Rock $\rho_r^{SO_4} = \sum_{i=1}^{3} \chi^i_{Salado}\chi_i^{SO_4}$			69.799

1. $\rho_{halite} = 2160 \text{ kg m}^{-3}$

3.2 Advective and Diffusive Transport of Sulfate

Estimates for the biodegradation time scale, advective sulfate transport and diffusive sulfate transport are presented below.

3.2.1 Time Scale

Figures 4 and 5 show the fraction of CPR remaining in the repository (BRAGFLO output variable CELL_REM) as a function of time obtained from the AMW S1 (undisturbed) and AMW S2 (E1 intrusion) scenario BRAGFLO simulations, respectively. The CDB files (ALG2_AMW_R1_S1_V###.CDB and ALG2_AMW_R1_S2_V###.CDB) containing the data for these plots are stored in the CMS libraries LIBAMW_BFR1S1 and LIBAMW_BFR1S2, respectively. The SUMMARIZE and SPLAT input files used to tabulate and plot the data are listed in Appendix A.

In all but a few vectors, CPR biodegradation has ceased after about 2000 years. In most vectors, this is because all of the CPR has been consumed. For a few vectors the consumption of CPR has ceased even though there is CPR remaining. This is likely caused by very low brine saturations. For those few vectors that still show some activity, the rate of CPR consumption is only a fraction of the inundated rate. Thus, a value 2000 years for the biodegradation time scale T_{bio} is appropriate for this analysis.

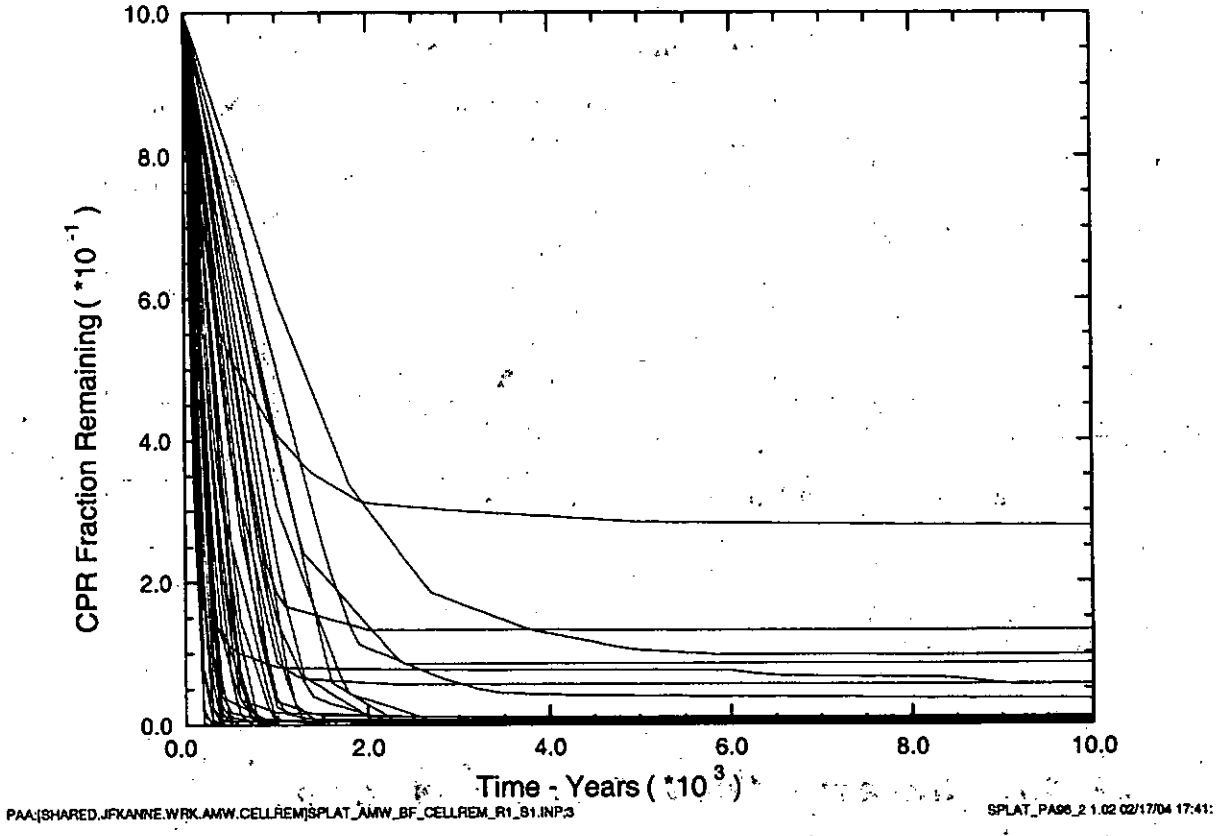

Figure 4. CPR Remaining in Repository (AMW R1 S1)

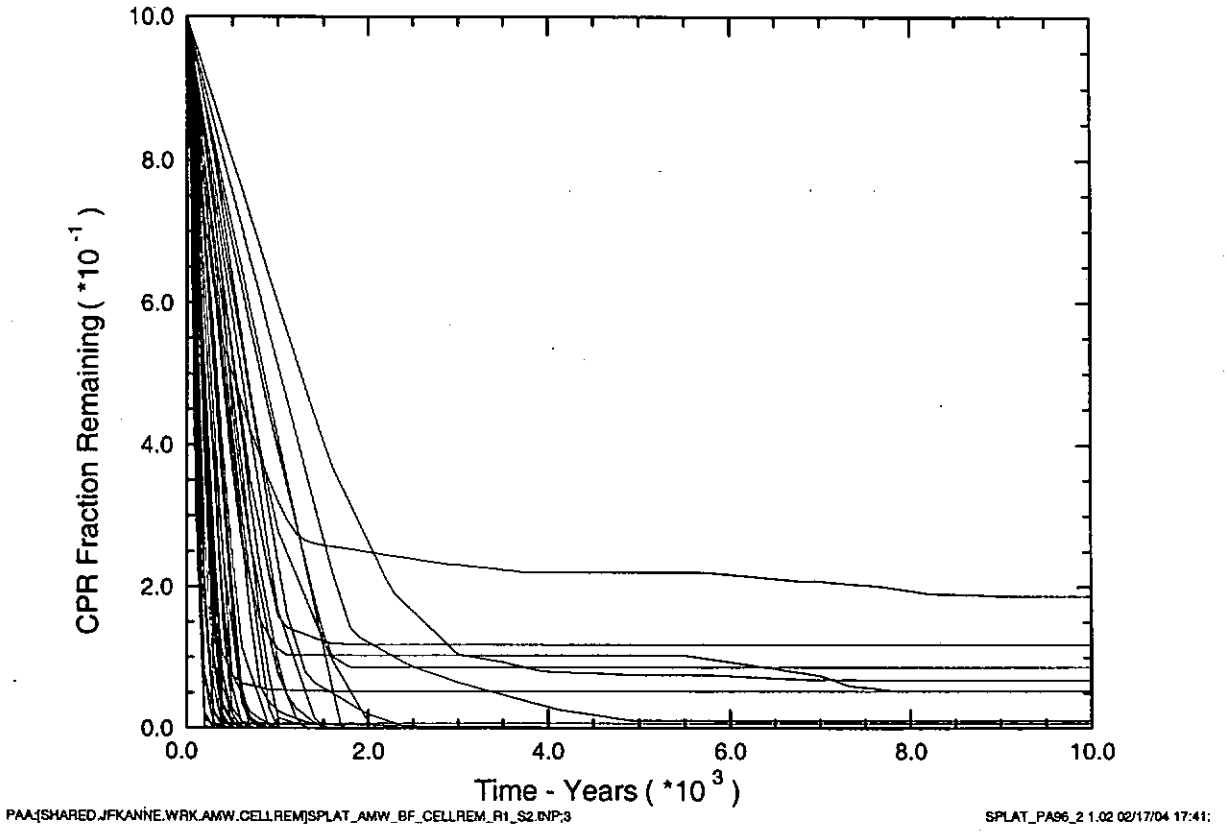

Figure 5. CPR Remaining in Repository (AMW R1 S2)

3.2.2 Advection of Sulfate in Brines

Table 7 shows the maximum cumulative brine inflow for panel X at 2000 years over all of the AMW BRAGFLO simulations (Replicate 1, Scenarios S1-S6, Vectors 1-100). As expected, the maximum brine flow into the panel occurs in a scenario with an E1 drilling intrusion. Also shown is the amount of sulfate advected in that brine volume calculated using Eq. 2.6, assuming the concentration of sulfate in the brine is 17.483 kg m^{-3}.

Table 7. Sulfate Advected into Panel X by Brine Inflows

Time Scale T (years)	Maximum Cumulative Brine Inflow		Sulfate Concentration in Brine $C_b^{SO_4}$ (kg m^{-3})	Sulfate Advected in Brine $M_b^{SO_4}$ (kg)
	AMW Vector	Volume V_b^{max} (m^3)		
2000	R1 S2 V046	7.74×10^4	17.483	1.35×10^6

3.2.3 Dissolution and Diffusion of Sulfate from the DRZ

Table 8 shows the effective diffusion coefficient calculated using the approach described in Section 2.3. The free liquid diffusion coefficient for sulfate in sea water (Li and Gregory 1974) is used for $D_0^{SO_4}$. The bounding value for DRZ porosity selected for this analysis is 0.05, the maximum allowable DRZ porosity used in BRAGFLO modeling (see the variable PHIMAX in BRAGFLO input files BF1_CRA1_S#.INP in CMS library LIBCRA1_BF) The tortuosity is calculated by substituting this porosity and the cementation factor proposed by (Deal et al. 1989) into Eq. 2.20. Finally, the effective diffusion coefficient is calculated using Eq. 2.10.

Table 8. Effective Diffusion Coefficient of Sulfate in DRZ

Free Liquid Diffusion Coefficient $D_0^{SO_4}$ ($m^2\ s^{-1}$)	Porosity ϕ (-)	Cementation Factor m (-)	Tortuosity τ (-)	Effective Diffusion Coefficient $D_{eff}^{SO_4}$ ($m^2\ s^{-1}$)
9.84×10^{-10}	0.05	1.8	9.1×10^{-2}	4.48×10^{-12}

The amount of sulfate in DRZ minerals that could possibly dissolve and diffuse into the waste rooms over a 2000 year time period, calculated using the approach outlined in Section 2.3, is shown in Table 9. The diffusion length is calculated from the time scale and the effective diffusion coefficient using Eq. 2.17. The total surface area of the waste panel is obtained from the grid used in the DBR simulations. The description of this grid is documented in its GENMESH input file (GM_DBR_CRA1.INP) available in the CMS library LIBCRA1_GM. The volume of rock within the diffusion length is calculated using Eq. 2.7. The amount of sulfate is calculated with the volume of rock and the average sulfate density from Table 6, using Eq. 2.8.

Table 9. Sulfate Transported into Panel X by Dissolution of Sulfate-bearing Minerals and Diffusion through DRZ

Time Scale T (years)	Effective Diffusion Coefficient $D_{eff}^{SO_4}$ ($m^2\ s^{-1}$)	Diffusion Length $L_{diff}^{SO_4}$ (m)	Panel Surface Area S_{rep} (m^2)	Rock Volume V_r (m^3)	Sulfate Density in DRZ Rock $\rho_{Salado}^{SO_4}$ (kg m^{-3})	Sulfate Diffused from DRZ Rock $M_r^{SO_4}$ (kg)
2000	4.48×10^{-12}	1.06	3.19×10^4	3.40×10^4	69.799	2.37×10^6

3.3 Effect of Sulfate on CPR Biodegradation and MgO Safety factor

Table 10 presents the total amount of sulfate available from all sources for each scenario. The amount of sulfate provided by advection and diffusion is typically two orders of magnitude larger than the sulfate in the waste. One observes that the largest sulfate contribution comes from diffusion, which is approximately double that from advection. The total amount of sulfate available is approximately equal for the four scenarios because they only differ by the amount of waste-derived sulfate. However, one should not expect the MgO safety factors to be equal because the amount of CPR varies considerably with the emplacement scenario.

Table 10. Total Sulfate Available in Panel X

Scenario	Sulfate Contained in Waste $M_w^{SO_4}$ (kg)	Sulfate Advected in Brine $M_b^{SO_4}$ (kg)	Sulfate Diffused from DRZ Rock $M_r^{SO_4}$ (kg)	Total Sulfate Available $M_{total}^{SO_4}$ (kg)
SNL Homogeneous	4.40×10^4	1.35×10^6	2.37×10^6	3.77×10^6
SNL Realistic	3.90×10^4	1.35×10^6	2.37×10^6	3.76×10^6
SNL Conservative	1.40×10^4	1.35×10^6	2.37×10^6	3.74×10^6
EPA Conservative	2.63×10^4	1.35×10^6	2.37×10^6	3.75×10^6

The amount of CPR consumed by each biodegradation pathway and the resulting MgO safety factor was calculated in the Microsoft Excel Workbooks shown in Table 11. These spreadsheets are available in Snider and Kanney (2004).

Table. 11 Microsoft Excel Workbooks for MgO Safety Factor Calculations

Scenario	Microsoft Excel Workbook
SNL Homogeneous	SNLhomogeneous_panelX_SO4_baseline.xls
SNL Realistic	SNLrealistic_panelX_SO4_baseline.xls
SNL Conservative	SNLconservative_panelX_SO4_baseline.xls
EPA Conservative	EPAconservative_panelX_SO4_baseline.xls
EPA Conservative (Waste Only)	EPAconservative_panelX_SO4_waste_only.xls

Table 12 summarizes the amount of CPR consumed by each biodegradation pathway and the resulting MgO safety factor given the estimates of waste-associated and naturally occurring sulfate. Results are provided for the SNL homogeneous panel X, the SNL realistic panel X, SNL conservative panel X, and the EPA conservative panel X. Previous results for the homogeneous 10-panel repository, SNL realistic panel X, and SNL conservative panel X which considered only waste-derived sulfate are included for comparison (Snider 2003a). Also included are the results for the EPA conservative panel X with only waste-derived sulfate.

Table 12. MgO Safety Factor for Panel X: Effect of Naturally Occurring Sulfate and Waste Emplacement Scenario

Scenario	Denitrification (%)	Sulfate Reduction (%)	Methanogenesis (%)	MgO Safety Factor (-)
SNL Homogeneous				
Waste + Natural Sulfate	4.75	70.57	24.68	1.37
Waste Sulfate Only[1]	4.75	0.82	94.46	2.45
SNL Realistic				
Waste + Natural Sulfate	4.48	63.27	32.26	1.40
Waste Sulfate Only[2]	4.48	0.66	94.87	2.44
SNL Conservative				
Waste + Natural Sulfate	3.00	42.98	54.03	1.13
Waste Sulfate Only[2]	3.00	0.16	96.84	1.71
EPA Conservative				
Waste + Natural Sulfate	1.03	32.31	66.66	0.94
Waste Sulfate Only	1.03	0.23	98.75	1.21

1 Homogeneous 10-panel repository (Snider 2003a)
2 (Hansen and Snider 2004)

The results in Table 12 show that, for a given emplacement scenario (i.e., for a given amount of CPR), accounting for transport of naturally occurring sulfate into the panel decreases the MgO safety factor relative to previous analyses which only considered sulfate in the waste. The MgO safety factor for the SNL homogeneous panel X is 1.37, compared to 2.45 for previous estimates for the homogeneous 10-panel repository. For the SNL realistic and conservative cases the safety factor dropped from 2.44 to 1.40 and from 1.71 to 1.13, respectively, when naturally occurring sulfate is included in the calculations. For the EPA conservative scenario, the safety factor decreases from 1.21 to 0.94.

In spite of the decreases noted above, these results show that the MgO safety factor is not very sensitive to the amount of sulfate. For the SNL homogeneous panel X, the amount of sulfate increased by about 8500% while the MgO safety factor decreased by about 44%. For the SNL realistic panel X, the amount of sulfate increased by about 9500% and the safety factor decreased by about 43%. For the SNL conservative case, the amount of sulfate increased by about 26,500% and the safety factor decreased by about 34%. For the EPA conservative scenario, the amount of sulfate increased by about 14000% and the MgO safety factor decreased by about 22%.

The MgO safety factor is much more sensitive to the amount of CPR. Keeping in mind that there is roughly the same amount of sulfate available in each scenario, one can observe how the safety factor changes as more CPR is added by comparing safety factors for different scenarios. In going from the SNL realistic case to the EPA conservative case, the CPR mass increases by about 95% and the MgO safety factor decreases by about 33%.

Note that the fraction of CPR degraded by sulfate reduction in the EPA conservative panel X scenario is actually less than for the SNL conservative panel X, while the MgO safety factor is lower than that of SNL conservative panel X. This is the caused by the larger amount of CPR in the EPA conservative panel X scenario.

4 Uncertainty Analysis

It is understood that an analysis such as presented here will always involve some level of uncertainty with respect to system parameters and future events. In order to provide a degree of confidence that the results presented in Section 3 represent a very conservative estimate on the amount of sulfate that might be available to participate in sulfate reduction, we identify and analyze sources of uncertainty in the calculations. Uncertain variables that will be discussed include brine volume, time scale, and effective diffusion coefficient.

4.1 Brine Volume

Although advection of sulfate in brine flowing through fractures has been much discussed, the fact is that BRAGFLO modeling consistently predicts that the largest brine inflows are associated with drilling intrusions that penetrate a theoretical pressurized brine pocket in the Castile Formation underlying the repository. The analysis presented here addresses this situation. However, the estimate for advective sulfate flux is based on the maximum brine inflow observed for any PA realization, and the probability of this worst-case scenario is quite small. It depends upon: 1) having at least one intrusion during the biodegradation time scale; 2) the intrusion hitting brine; 3) having a large brine flow from the Castile; and 4) the borehole having a 2-plug configuration. Table 13 summarizes the probabilities of these events and the resulting probability of the largest brine inflow, which is less than one percent.

Table 13. Probability of Large Brine Inflow Due to Intrusion

Event	Description	Probability
1	At least one intrusion into CH waste between 100 and 2000 years	[a]0.67
2	Intrusion hits brine in the Castile	[b]0.59
3	Two-plug configuration in borehole	[c]0.70
4	Large brine flow from Castile	[d]0.10
5	Intrusion into panel with 50% supercompacted waste	[e]0.20
	Probability of events A through E coinciding $\left(\prod_{i=1}^{5} P_i\right)$	0.006

a. $P(0 \text{ boreholes by } 2000 \text{ years}) = e^{-\lambda t}$ where $\lambda = 5.8 \times 10^{-4}$ (Dunagan 2003), and $t = 1900$ years.
$P(1 \text{ borehole by } 2000 \text{ years}) = 1 - P(0 \text{ boreholes by } 2000 \text{ years})$.

b. 0.99 quantile of variable uniformly distributed between 0.01 and 0.6

c. The probability of having the 2 plug configuration is 0.696. The solid plug and the three plug configurations are assumed to prevent flow from the Castile upwards.

d. Approximately 10 % of PA vectors have large brine flows.

e. The worst case waste loading assumes that 50% of panel's volume is filled with supercompacted waste (about 8500 m3) Since there is about 19,000 m3 of supercompacted waste, only 2 of 10 panels can be filled.

Since the large brine flows have such a low probability of occurrence, one should consider what the MgO safety factor would be if they are absent. We can easily estimate this by calculating the MgO safety factor using the maximum brine inflow over all vectors in scenarios where an E1 intrusion does not occur (i.e. S1, S4, and S5). Table 14 shows that the

maximum amount of sulfate advected into a panel in the absence of E1 intrusions is only about 25% of that seen in the baseline case where an E1 intrusion occurs. Table 15 shows that the total amount of sulfate available is about 73% of that available in the baseline case.

Table 14. Effect of No E1 Intrusion of Sulfate Advection in Panel X

Time Scale T_{bio} (years)	Maximum Cumulative Brine Inflow		Sulfate Concentration in Brine $C_b^{SO_4}$ (kg m^{-3})	Sulfate Advected in Brine $M_b^{SO_4}$ (kg)
	AMW Vector	Volume V_b^{max} (m^3)		
2000	R1 S4 V091	1.91×10^4	17.483	3.34×10^5
2000	R1 S2 V046	7.74×10^4	17.483	1.35×10^6

Table 15. Effect of No E1 Intrusion on Available Sulfate in Panel X

Scenario	Sulfate Contained in Waste $M_w^{SO_4}$ (kg)	Sulfate Advected in Brine $M_b^{SO_4}$ (kg)	Sulfate Diffused from DRZ Rock $M_r^{SO_4}$ (kg)	Total Sulfate Available $M_{total}^{SO_4}$ (kg)
SNL Homogeneous				
No E1 Intrusion	4.40×10^4	3.33×10^5	2.37×10^6	2.75×10^6
Baseline	4.40×10^4	1.35×10^6	2.37×10^6	3.77×10^6
SNL Realistic				
No E1 Intrusion	3.90×10^4	3.33×10^5	2.37×10^6	2.74×10^6
Baseline	3.90×10^4	1.35×10^6	2.37×10^6	3.76×10^6
SNL Conservative				
No E1 Intrusion	1.40×10^4	3.33×10^5	2.37×10^6	2.72×10^6
Baseline	1.40×10^4	1.35×10^6	2.37×10^6	3.74×10^6
EPA Conservative				
No E1 Intrusion	2.63×10^4	3.33×10^5	2.37×10^6	2.73×10^6
Baseline	2.63×10^4	1.35×10^6	2.37×10^6	3.75×10^6

The effect of no E1 intrusions on the MgO safety factor for the SNL homogeneous panel X, SNL realistic panel X, SNL conservative panel X, and EPA conservative panel X emplacement scenarios were calculated the Excel Workbooks shown in Table 16. These spreadsheets are available in Snider and Kanney (2004). Results of these calculations are shown in Table 17. One observes that the MgO safety factor increases by approximately

11% in the SNL homogeneous and SNL realistic scenarios and by 8% and 6% in the SNL conservative and EPA conservative cases, respectively. The decreasing change in safety factor reflects the increasing amounts of CPR in these emplacement scenarios.

Table 16. Microsoft Excel Workbooks for MgO Safety Factor Calculations: Effect of No E1 Intrusions

Scenario	Microsoft Excel Workbook
SNL Homogeneous	SNLhomogeneous_panelX_SO4_A.xls
SNL Realistic	SNLrealistic_panelX_SO4_A.xls
SNL Conservative	SNLconservative_panelX_SO4_A.xls
EPA Conservative	EPAconservative_panelX_SO4_A.xls

Table 17. Effect of No E1 Intrusion on MgO Safety Factor in Panel X

Scenario	Denitrification (%)	Sulfate Reduction (%)	Methanogenesis (%)	MgO Safety Factor (-)
SNL Homogeneous				
No E1 Intrusion	4.75	51.47	43.77	1.52
Baseline	4.75	70.57	24.68	1.37
SNL Realistic				
No E1 Intrusion	4.48	46.13	49.40	1.55
Baseline	4.48	63.27	32.26	1.40
SNL Conservative				
No E1 Intrusion	3.00	31.26	65.75	1.22
Baseline	3.00	42.98	54.03	1.13
EPA Conservative				
No E1 Intrusion	1.03	23.53	75.44	1.00
Baseline	1.03	32.31	66.66	0.94

4.2 Time Scale

If the time scale over which biodegradation occurs is larger than the estimate presented in Section 3.2.2, it would allow more time for advection and diffusion of sulfate to occur. In order to evaluate the sensitivity of the MgO safety factor to the time scale, we can calculate

the available sulfate and corresponding MgO safety factor for a time scale twice as long as used in the baseline case

Table 18 shows that doubling the time scale increases the brine volume and the amount of sulfate advected into the panel by a factor of approximately 1.3. As before, the maximum brine inflow occurs in a scenario that includes an E1 drilling intrusion. Table 19 shows that doubling the time scale increases the diffusion length and the amount of sulfate diffused into the panel by a factor of approximately 1.4. Note that according to Eq. 2.17, the diffusive mass transfer will increase like the square root of the time scale increase. Table 20 shows that doubling the time scale increases the total amount of available sulfate by a factor of approximately 1.37.

Table 18. Sulfate Advection into Panel X: Effect of Doubling Time Scale

Time Scale	Maximum Cumulative Brine Inflow		Sulfate Concentration in Brine	Sulfate Advected in Brine
	AMW Vector	Volume		
T_{bio} (years)		V_b^{max} (m^3)	$C_b^{SO_4}$ (kg m^{-3})	$M_b^{SO_4}$ (kg)
4000	R1 S6 V046	1.02×10^5	17.483	1.78×10^6
2000	R1 S2 V046	7.74×10^4	17.483	1.35×10^6

Table 19. Sulfate Dissolution and Diffusion into Panel X: Effect of Doubling Time Scale

Time Scale	Effective Diffusion Coefficient	Diffusion Length	Panel Surface Area	Rock Volume	Sulfate Density in DRZ Rock	Sulfate Diffused from DRZ Rock
T_{bio} (years)	$D_{eff}^{SO_4}$ (m^2 s^{-1})	$L_{diff}^{SO_4}$ (m)	S_{rep} (m^2)	V_r (m^3)	$\rho_{Salado}^{SO_4}$ (kg m^{-3})	$M_r^{SO_4}$ (kg)
4000	4.48×10^{-12}	1.50	3.19×10^4	4.80×10^4	69.799	3.35×10^6
2000	4.48×10^{-12}	1.06	3.19×10^4	3.40×10^4	69.799	2.37×10^6

Table 20. Total Sulfate Available in Panel X: Effect of Doubling Time Scale

Scenario	Sulfate Contained in Waste $M_w^{SO_4}$ (kg)	Sulfate Advected in Brine $M_b^{SO_4}$ (kg)	Sulfate Diffused from DRZ Rock $M_r^{SO_4}$ (kg)	Total Sulfate Available $M_{total}^{SO_4}$ (kg)
SNL Homogeneous				
Increased Time Scale	4.40×10^4	1.78×10^6	3.35×10^6	5.17×10^6
Baseline	4.40×10^4	1.35×10^6	2.37×10^6	3.77×10^6
SNL Realistic				
Increased Time Scale	3.90×10^4	1.78×10^6	3.35×10^6	5.17×10^6
Baseline	3.90×10^4	1.35×10^6	2.37×10^6	3.76×10^6
SNL Conservative				
Increased Time Scale	1.40×10^4	1.78×10^6	3.35×10^6	5.14×10^6
Baseline	1.40×10^4	1.35×10^6	2.37×10^6	3.74×10^6
EPA Conservative				
Increased Time Scale	2.63×10^4	1.78×10^6	3.35×10^6	5.15×10^6
Baseline	2.63×10^4	1.35×10^6	2.37×10^6	3.75×10^6

The effects of additional sulfate from a doubling of the biodegradation time scale on the MgO safety factor for the SNL homogeneous panel X, SNL realistic panel X, SNL conservative panel X, and EPA conservative panel X emplacement scenarios were calculated the in Excel Workbooks as shown in Table 21. These spreadsheets are available in Snider and Kanney (2004). Results of these calculations are shown in Table 22. A factor of 2 increase in the time scale results in modest reductions in the safety factor. The MgO safety factor decreases by about 10%, 9%, 8% and 6% in the SNL homogeneous, SNL realistic, SNL conservative, and EPA conservative scenarios, respectively.

Table 21. Microsoft Excel Workbooks for MgO Safety Factor Calculations: Effect of Doubling Time Scale

Scenario	Microsoft Excel Workbook
SNL Homogeneous	SNLhomogeneous_panelX_SO4_B.xls
SNL Realistic	SNLrealistic_panelX_SO4_B.xls
SNL Conservative	SNLconservative_panelX_SO4_B.xls
EPA Conservative	EPAconservative_panelX_SO4_B.xls

Table 22. MgO Safety Factor in Panel X: Effect of Doubling Time Scale

Scenario	Denitrification (%)	Sulfate Reduction (%)	Methanogenesis (%)	MgO Safety Factor (-)
SNL Homogeneous				
Increased Time Scale	4.75	95.25	0.00	1.21
Baseline	4.75	70.57	24.68	1.37
SNL Realistic				
Increased Time Scale	4.48	86.98	8.54	1.25
Baseline	4.48	63.27	32.26	1.40
SNL Conservative				
Increased Time Scale	3.00	59.20	37.81	1.02
Baseline	3.00	42.98	54.03	1.13
EPA Conservative				
Increased Time Scale	1.03	44.47	54.51	0.86
Baseline	1.03	32.31	66.66	0.94

4.3 Dissolution and Diffusion

In order to evaluate the sensitivity of the MgO safety factor estimates to the effective diffusion coefficient, we can calculate the available sulfate and corresponding MgO safety factor for an effective diffusion coefficient 2 times larger than that considered in the baseline case. The effect on available sulfate of a twofold increase in the diffusion coefficient is shown in Table 23. As indicated in Eq. 2.17, the increase in sulfate available from the DRZ scales like the square root of the change in the diffusion coefficient. The total amount of sulfate available, shown in Table 24, increases by a factor of approximately 1.3 compared to the baseline values.

Table 23. Sulfate Dissolution and Diffusion into Panel X: Effect of Doubling Effective Diffusion Coefficient

Time Scale T_{bio} (years)	Effective Diffusion Coefficient $D_{eff}^{SO_4}$ ($m^2\ s^{-1}$)	Diffusion Length $L_{diff}^{SO_4}$ (m)	Panel Surface Area S_{rep} (m^2)	Rock Volume V_r (m^3)	Sulfate Density in DRZ Rock $\rho_{Salado}^{SO_4}$ ($kg\ m^{-3}$)	Sulfate Diffused from DRZ Rock $M_r^{SO_4}$ (kg)
2000	1.00×10^{-11}	1.59	3.19×10^4	5.08×10^4	69.799	3.54×10^6
2000	4.48×10^{-12}	1.06	3.19×10^4	3.40×10^4	69.799	2.37×10^6

Table 24. Total Sulfate Available in Panel X: Effect of Doubling Effective Diffusion Coefficient

Scenario	Sulfate Contained in Waste $M_w^{SO_4}$ (kg)	Sulfate Advected in Brine $M_b^{SO_4}$ (kg)	Sulfate Diffused from DRZ Rock $M_r^{SO_4}$ (kg)	Total Sulfate Available $M_{total}^{SO_4}$ (kg)
SNL Homogeneous				
Increased Diffusion	4.40×10^4	1.35×10^6	3.54×10^6	4.94×10^6
Baseline	4.40×10^4	1.35×10^6	2.37×10^6	3.77×10^6
SNL Realistic				
Increased Diffusion	3.90×10^4	1.35×10^6	3.54×10^6	4.94×10^6
Baseline	3.90×10^4	1.35×10^6	2.37×10^6	3.76×10^6
SNL Conservative				
Increased Diffusion	1.40×10^4	1.35×10^6	3.54×10^6	4.91×10^6
Baseline	1.40×10^4	1.35×10^6	2.37×10^6	3.74×10^6
EPA Conservative				
Increased Diffusion	2.63×10^4	1.35×10^6	3.54×10^6	4.92×10^6
Baseline	2.63×10^4	1.35×10^6	2.37×10^6	3.75×10^6

The effects of additional sulfate from doubling the effective diffusion coefficient on the MgO safety factor for the SNL homogeneous panel X, SNL realistic panel X, SNL conservative panel X, and EPA conservative panel X emplacement scenarios were calculated in the Excel workbooks shown in Table 25. These spreadsheets are available in Snider and Kanney (2004). Results of these calculations are shown in Table 26. The impact of doubling the

effective diffusion coefficient is similar to doubling the time scale. This is reasonable given that that dissolution and diffusion contribute the most sulfate and diffusive transport scales like the square root of time as well as the square root of diffusion coefficient. We note doubling the effective diffusion coefficient results in modest decreases in the MgO safety factor (10 to 6%) relative to the baseline case. As before, the change in MgO safety factor decreases with increasing amounts of CPR in the panel scenario.

Table 25 Microsoft Excel Workbooks for MgO Safety Factor Calculations: Effect of Doubling Effective Diffusion Coefficient

Scenario	Microsoft Excel Workbook
SNL Homogeneous	SNLhomogeneous_panelX_SO4_C.xls
SNL Realistic	SNLrealistic_panelX_SO4_C.xls
SNL Conservative	SNLconservative_panelX_SO4_C.xls
EPA Conservative	EPAconservative_panelX_SO4_C.xls

Table 26. MgO Safety Factor in Panel X: Effect of Doubling Effective Diffusion Coefficient

Scenario	Denitrification (%)	Sulfate Reduction (%)	Methanogenesis (%)	MgO Safety Factor (-)
SNL Homogeneous				
Increased Diffusion	4.75	92.48	2.76	1.23
Baseline	4.75	70.57	24.68	1.37
SNL Realistic				
Increased Diffusion	4.48	82.94	12.58	1.27
Baseline	4.48	63.27	32.26	1.40
SNL Conservative				
Increased Diffusion	3.00	56.44	40.57	1.04
Baseline	3.00	42.98	54.03	1.13
EPA Conservative				
Increased Diffusion	1.03	42.40	56.58	0.88
Baseline	1.03	32.31	66.66	0.94

5 Summary and Conclusions

This analysis provides a very conservative estimate of the amount of naturally occurring sulfate that could be available to participate in the CPR biodegradation, based upon the combined effect of many conservative assumptions that are incorporated into the analysis. These conservatisms include:

- The sulfate concentration in brine is assumed to be the maximum over all of the model brines.
- The average mineralogy model neglects the presence of clays, overestimating the amount of sulfate-bearing minerals in the Salado.
- The estimates of advective sulfate flux are based on the maximum observed brine flow over all PA realizations. The maximum volume used has a very low probability of occurrence.
- The diffusion model assumes that the DRZ is fully saturated. In reality, large portions of the DRZ will be only partially saturated for most of the regulatory period. Diffusion rates in partially saturated porous media are considerably less than in saturated media.
- The estimates of sulfate diffusion assume that the DRZ porosity is equal to the maximum BRAGFLO DRZ porosity for the entire time period over which diffusion operates.
- The assumption that all sulfate-bearing minerals within the proposed diffusion length dissolve and are transported into the waste panels is obviously conservative because it completely neglects mass transfer limitations in the mineral dissolution process.

In the baseline estimate developed in this analysis, the safety factor for the homogeneous panel X, SNL realistic panel X, SNL conservative panel X, and the EPA conservative panel X scenarios is 1.37, 1.40, 1.13, and 0.94, respectively. Thus, even under the very conservative assumptions of this analysis, the MgO safety factor calculated on a panel basis is larger than 1.0 in all but the EPA conservative case. More realistic modeling, i.e., not limited to bounding analyses, would increase these values considerably.

The results obtained in this analysis show that the MgO safety factor is a function of both the sulfate available and the emplacement scenario. The MgO safety factor is shown to be more sensitive to the emplacement scenario (i.e., to the amount of CPR present) than to the amount of sulfate present. This analysis indicates that dissolution and diffusion of sulfate into the waste panel is the main source of naturally occurring sulfate, although this may largely a function of the conservatism used in the modeling.

The uncertainty analysis presented in Section 4 addressed the effects of brine volume, time scale and effective diffusion coefficient on the MgO safety factor. Results show that the MgO safety factor is only moderately sensitive to these variables, and that their impact decreases as more CPR is added to a panel.

Because of the low probability of large brine flows, MgO safety factors were calculated for the case where there is no E1 intrusion. In the absence of an E1 intrusion, the sulfate advected in brines decrease by a factor of 4 while the total sulfate available decreases by a factor of about 0.75. In response, MgO safety factors increase by 6 to 11%. The smallest change was calculated for the EPA conservative panel X scenario, which has the largest CPR content. The largest change was calculated for the SNL homogeneous panel X scenario, which has the lowest CPR content.

Doubling the biodegradation time scale increases the total amount of sulfate by a factor of 1.3 and decreases MgO safety factors by 6 to 10%. The smallest change was calculated for the EPA conservative panel X scenario, which has the largest CPR content. The largest change was calculated for the SNL homogeneous panel X scenario, which has the lowest CPR content.

Doubling the effective diffusion coefficient increases the total amount of sulfate by a factor of 1.3 and decreases the MgO safety factors by 6 to 10%. The smallest change was calculated for the EPA conservative panel X scenario, which has the largest CPR content. The largest change was calculated for the SNL homogeneous panel X scenario, which has the lowest CPR content.

6 References

Abramowitz, M., and I. Stegun. 1972. Handbook of Mathematical Functions. Dover, New York.

Archie, G. E. 1942. The Electrical Resisitivity Log as an Aid in Determining Some Reservoir Characteristics. Transactions of the American Institute of Mining Engineers **146**:54-62.

Brush, L. H. 1990. Test Plan for Laboratory and Modeling Studies of Repository and Radionuclide Chemistry for the Waste Isolation Pilot Plant. Sandia Report SAND90-0266, Sandia National Laboratories, Albuquerque, NM.

Brush, L. H., and Y. Xiong. 2003a. Calculation of Actinide Solubilities for the WIPP Compliance Recertification Application. Analysis Report ERMS 527714, Sandia National Laboratories, Carlsbad, NM.

Brush, L. H., and Y. Xiong. 2003b. Calculation of Actinide Solubilities for the WIPP Compliance Recertification Application, Analysis Plan AP-098, Rev 1. Analysis Plan ERMS 527714, Sandia National Laboratories, Carlsbad, NM.

Costin, L. S., and W. R. Wawersik. 1980. Crack Healing of Fractures in Rock Salt. Sandia Report SAND80-0392, Sandia National Laboratories, Albuquerque, NM.

Cussler, E. L. 1997. Diffusion: Mass Transfer in Fluid Systems, Second edition. Cambridge University Press, New York.

de Marsily, G. 1986. Quantitative Hydrogeology. San Diego, Academic Press.

Deal, D. E., R. J. Abitz, D. S. Belski, J. B. Case, M. E. Crawley, R. M. Deshler, P. E. Drez, C. A. Givens, R. B. King, B. A. Lauctes, J. Myers, S. Niou, J. M. Pietz, W. M. Roggenthen, J. R. Tyburski, and M. G. Wallace. 1989. Brine Sampling and Evaluation Program 1988 Report. DOE-WIPP-98-015, Westinghouse Electric Corporation, Waste Isolation Division, Carlsbad, NM.

Deal, D. E., R. J. Abitz, D. S. Belski, J. B. Case, M. E. Crawley, C. A. Givens, P. P. J. Lipponer, J. Myers, D. W. Powers, and M. A. Valdiva. 1995. Brine Sampling and Evaluation Program 1992-1993 Report and Summary of BSEP Data Since 1982. Contractor Report DOE-WIPP 94-011, U.S. Department of Energy WIPP Project Office, Carlsbad, NM.

Dunagan, S. 2003. Estimated Number of Boreholes into CH Waste in 10,000 Years. Technical Memorandum ERMS 532277, Sandia National Laboratories, Carlsbad, NM.

Francis, A. J., J. B. Gillow, and M. R. Giles. 1997. Microbial Gas Generation Under Expected Waste Isolation Pilot Plant Repository Conditions. Contractor Report SAND96-2582, Sandia National Laboratories, Albuquerque, NM.

Freeze, R. A., and J. Cherry. 1979. Groundwater. Prentice-Hall, Englewood Cliffs, NJ.

Hansen, C. W., L. H. Brush, M. B. Gross, F. D. Hansen, B. Y. Park, J. S. Stein, and T. W. Thompson. 2004. Effects of Supercompacted Waste and Heterogeneous Waste Emplacement on Repository Performance, Revision 2. Analysis Report ERMS 533551, Sandia National Laboratories, Carlsbad, NM.

Hansen, C. W., and A. C. Snider. 2004. Effect of TDOP Stacking Assumptions on Analysis of Supercompacted Waste, Revision 1. Technical Memorandum ERMS 534043, Sandia National Laboratories, Carlsbad, NM.

Hansen, F. D. 2003. The Disturbed Rock Zone at the Waste Isolation Pilot Plant. Sandia Report SAND2003-3407, Sandia National Laboratories, Albuquerque, NM.

Helton, J. C., J. E. Bean, F. W. Berglund, F. J. Davis, K. Economy, J. W. Garner, J. D. Johnson, R. J. MacKinnon, J. Miller, D. G. O'Brien, J. L. Ramsey, J. D. Schreiber, A. Shinta, L. N. Smith, D. M. Stoelzel, C. Stockman, and P. Vaughn. 1998. Uncertainty and Sensitivity Analysis Results Obtained in the 1996 Performance Assessment for the Waste Isolation Pilot Plant. Sandia Report SAND98-0365, Sandia National Laboratories, Albuquerque, NM.

Leigh, C. D. 2003. Estimate of Cellulosics, Plastics and Rubbers in a Single Panel in the WIPP Repository in Support of AP-107, Revision 1. Analysis Report ERMS 531324, Sandia National Laboratories, Carlsbad, NM.

Leigh, C. D. 2004a. Waste Parameters for a Single Panel Assuming a 50/50 Volume Split Between INEEL Supercompacted Waste and Waste from Other Sites, Revision 1. Technical Memorandum ERMS 534016, Sandia National Laboratories, Carlsbad, NM.

Leigh, C. D. 2004b. Waste Parameters for an Alternative TDOP Loading Assumption in the AMW Analysis, Revision 1. Technical Memorandum ERMS 534017, Sandia National Laboratories, Carlsbad, NM.

Li, Y. H., and S. Gregory. 1974. Diffusion of Ions in Sea Water and in Deep Sea Sediments. Geochimica et Cosmochimica Acta **38**:703-714.

Marcinowski, F. 2004. Letter to Paul Detwiler regarding the Department of Energy's request to dispose of supercompacted waste from the Idaho National Environment and Engineering Laboratory (INEEL) Advanced Mixed Waste Treatment Facility (AMWTF). EPA Correspondence ERMS 533934, U. S. Environmental Protection Agency, Washington, D.C.

Popielak, R. S., R. L. Beauheim, S. R. Black, W. E. Coons, C. T. Ellingson, and R. L. Olsen. 1983. Brine Reservoirs in the Castile Formation, Waste Isolation Pilot Plant (WIPP) Project, Southeastern New Mexico. TME-3153, U.S. Department of Energy Waste Isolation Pilot Plant, Albuquerque, NM.

Snider, A. C. 2003a. Calculation of MgO Safety Factors for the WIPP Compliance Recertification Application and for Evaluating Assumptions of Waste Heterogeneity in WIPP PA. Analysis Report ERMS 531508, Sandia National Laboratories, Carlsbad, NM.

Snider, A. C. 2003b. Verification of the Definition of Generic Weep Brine and the Development of a Recipe for This Brine. Analysis Report ERMS 527505, Sandia National Laboratories, Carlsbad, NM.

Snider, A. C., and J. F. Kanney. 2004. Microsoft Excel Spreadsheet Calculations for the Effect of Naturally Occurring Sulfate on MgO Safety Factor. Machine Readable Media Sandia National Laboratory, Carlsbad, NM.

Stein, C. L. 1985. Mineralogy in the Waste Isolation Pilot Plant (WIPP) Facility Stratigraphic Horizon. SAND85-0321, Sandia National Laboratories, Albuquerque, NM.

Stein, J. S., and W. Zelinski. 2003. Analysis Package for BRAGFLO: Compliance Recertification Application. Analysis Report ERMS 530163, Sandia National Laboratory, Carlsbad, NM.

Stumm, W., and J. J. Morgan. 1996. Aquatic Chemistry: Chemical Equilibria and Rates in Natural Waters, Third edition. John Wiley & Sons, New York.

Swift, P. N., and T. F. Corbet. 2000. The Geological and Hydrogeological Setting of the Waste Isolation Pilot Plant. Reliability Engineering and System Safety **69**:47-58.

U.S. DOE. 1983a. Results of Site Validation Experiments, Waste Isolation Pilot Plant (WIPP) Project, Southeastern New Mexico. Vol. I. Executive Summary, Text, and Supporting Documents 1 through 4. TME-3177, Vol. I, U.S. Department of Energy Waste Isolation Pilot Plant, Albuquerque, NM.

U.S. DOE. 1983b. Results of Site Validation Experiments, Waste Isolation Pilot Plant (WIPP) Project, Southeastern New Mexico. Vol. II. Supporting Documents 5 through 14. TME-3177, Vol. II, U.S. Department of Energy Waste Isolation Pilot Plant, Albuquerque, NM.

U.S. DOE. 1996. Title 40 CFR Part 191 Compliance Certification Application for the Waste Isolation Pilot. DOE/CAO-1996-2184, U.S. Department of Energy Waste Isolation Pilot Plant, Carlsbad Area Office, Carlsbad, NM.

Wang, Y., and L. H. Brush. 1996. Estimates of Gas Generation Parameters for the Long-Term WIPP Performance. Technical Memorandum ERMS 239143, Sandia National Laboratories, Carlsbad, NM.

WIPP PA. 1992. Preliminary Performance Assessment for the Waste Isolation Pilot Plant. Sandia Report SAND92-070, Sandia National Laboratories, Albuquerque, NM.

WIPP PA. 2003. BRAGFLO Version 5.00. WIPP PA User's Manual ERMS 525702, Sandia National Laboratories, Carlsbad, NM.

Appendix A Files for Time Scale Estimate

A.1 SUMMARIZE Input File (SUM_AMW_BF_CELLREM_R1_S1.INP)

```
*input files
template = alg2_amw_r1_s1_v###
directory = [.cdb]
type = CDB

*vector
id = #
vector = 1 to 100

*times
read = seconds
input = years
output = years
times = 0 to 10000 by 100

*items
type =global
name = cell_rem

*output
driver = SPLAT
write = time vs item
MULTIPLE_FILES
name = [.tbl]sum_amw_bf_bsat_r1_s1_v###
EXTENSION = TBL

*end
```

A.2 SPLAT Input File (SPLAT_AMW_BF_CELLREM_R1_S1.INP)

```
size text 0.017
title device 0.15,0.75 "AMW BF R1 S1: Fraction of CPR Remaining"
lstyle curve solid
axis linear
label "Time - Years","CPR Fraction Remaining "
width curve 0.5

overlay [.TBL]SUM_AMW_BF_CELLREM_R1_S1_V002.TBL 2,3
overlay [.TBL]SUM_AMW_BF_CELLREM_R1_S1_V004.TBL 2,3
overlay [.TBL]SUM_AMW_BF_CELLREM_R1_S1_V005.TBL 2,3
overlay [.TBL]SUM_AMW_BF_CELLREM_R1_S1_V006.TBL 2,3
overlay [.TBL]SUM_AMW_BF_CELLREM_R1_S1_V009.TBL 2,3
overlay [.TBL]SUM_AMW_BF_CELLREM_R1_S1_V010.TBL 2,3
overlay [.TBL]SUM_AMW_BF_CELLREM_R1_S1_V012.TBL 2,3
overlay [.TBL]SUM_AMW_BF_CELLREM_R1_S1_V014.TBL 2,3
overlay [.TBL]SUM_AMW_BF_CELLREM_R1_S1_V015.TBL 2,3
overlay [.TBL]SUM_AMW_BF_CELLREM_R1_S1_V016.TBL 2,3
overlay [.TBL]SUM_AMW_BF_CELLREM_R1_S1_V017.TBL 2,3
overlay [.TBL]SUM_AMW_BF_CELLREM_R1_S1_V018.TBL 2,3
overlay [.TBL]SUM_AMW_BF_CELLREM_R1_S1_V022.TBL 2,3
overlay [.TBL]SUM_AMW_BF_CELLREM_R1_S1_V023.TBL 2,3
overlay [.TBL]SUM_AMW_BF_CELLREM_R1_S1_V026.TBL 2,3
overlay [.TBL]SUM_AMW_BF_CELLREM_R1_S1_V027.TBL 2,3
overlay [.TBL]SUM_AMW_BF_CELLREM_R1_S1_V028.TBL 2,3
overlay [.TBL]SUM_AMW_BF_CELLREM_R1_S1_V029.TBL 2,3
overlay [.TBL]SUM_AMW_BF_CELLREM_R1_S1_V030.TBL 2,3
overlay [.TBL]SUM_AMW_BF_CELLREM_R1_S1_V034.TBL 2,3
overlay [.TBL]SUM_AMW_BF_CELLREM_R1_S1_V039.TBL 2,3
overlay [.TBL]SUM_AMW_BF_CELLREM_R1_S1_V040.TBL 2,3
overlay [.TBL]SUM_AMW_BF_CELLREM_R1_S1_V041.TBL 2,3
overlay [.TBL]SUM_AMW_BF_CELLREM_R1_S1_V042.TBL 2,3
overlay [.TBL]SUM_AMW_BF_CELLREM_R1_S1_V043.TBL 2,3
overlay [.TBL]SUM_AMW_BF_CELLREM_R1_S1_V045.TBL 2,3
overlay [.TBL]SUM_AMW_BF_CELLREM_R1_S1_V046.TBL 2,3
overlay [.TBL]SUM_AMW_BF_CELLREM_R1_S1_V047.TBL 2,3
overlay [.TBL]SUM_AMW_BF_CELLREM_R1_S1_V051.TBL 2,3
overlay [.TBL]SUM_AMW_BF_CELLREM_R1_S1_V052.TBL 2,3
overlay [.TBL]SUM_AMW_BF_CELLREM_R1_S1_V053.TBL 2,3
overlay [.TBL]SUM_AMW_BF_CELLREM_R1_S1_V064.TBL 2,3
overlay [.TBL]SUM_AMW_BF_CELLREM_R1_S1_V067.TBL 2,3
overlay [.TBL]SUM_AMW_BF_CELLREM_R1_S1_V068.TBL 2,3
overlay [.TBL]SUM_AMW_BF_CELLREM_R1_S1_V072.TBL 2,3
overlay [.TBL]SUM_AMW_BF_CELLREM_R1_S1_V073.TBL 2,3
overlay [.TBL]SUM_AMW_BF_CELLREM_R1_S1_V076.TBL 2,3
overlay [.TBL]SUM_AMW_BF_CELLREM_R1_S1_V077.TBL 2,3
overlay [.TBL]SUM_AMW_BF_CELLREM_R1_S1_V078.TBL 2,3
overlay [.TBL]SUM_AMW_BF_CELLREM_R1_S1_V079.TBL 2,3
overlay [.TBL]SUM_AMW_BF_CELLREM_R1_S1_V082.TBL 2,3
overlay [.TBL]SUM_AMW_BF_CELLREM_R1_S1_V085.TBL 2,3
overlay [.TBL]SUM_AMW_BF_CELLREM_R1_S1_V086.TBL 2,3
overlay [.TBL]SUM_AMW_BF_CELLREM_R1_S1_V087.TBL 2,3
overlay [.TBL]SUM_AMW_BF_CELLREM_R1_S1_V089.TBL 2,3
overlay [.TBL]SUM_AMW_BF_CELLREM_R1_S1_V090.TBL 2,3
overlay [.TBL]SUM_AMW_BF_CELLREM_R1_S1_V091.TBL 2,3
overlay [.TBL]SUM_AMW_BF_CELLREM_R1_S1_V093.TBL 2,3
overlay [.TBL]SUM_AMW_BF_CELLREM_R1_S1_V099.TBL 2,3
overlay [.TBL]SUM_AMW_BF_CELLREM_R1_S1_V100.TBL 2,3
replot 0,1E+4,0,1E+0,5,4,5,4
exit
```

A.3 SUMMARIZE Input File (SUM_AMW_BF_CELLREM_R1_S2.INP)

```
*input files
template = alg2_amw_r1_s2_v###
directory = [.cdb]
type = CDB

*vector
id = #
vector = 1 to 100

*times
read = seconds
input = years
output = years
times = 0 to 10000 by 100

*items
type =global
name = cell_rem

*output

driver = SPLAT
write = time vs item
MULTIPLE_FILES
name = [.tbl]sum_amw_bf_cellrem_r1_s2_v###
EXTENSION = TBL

*end
```

A.4 SPLAT Input File (SPLAT_AMW_BF_CELLREM_R1_S2.INP)

```
size text 0.017
title device 0.15,0.75 "AMW BF R1 S2: Fraction of CPR Remaining"
lstyle curve solid
axis linear
label "Time - Years","CPR Fraction Remaining "
width curve 0.5

overlay [.TBL]SUM_AMW_BF_CELLREM_R1_S2_V002.TBL 2,3
overlay [.TBL]SUM_AMW_BF_CELLREM_R1_S2_V004.TBL 2,3
overlay [.TBL]SUM_AMW_BF_CELLREM_R1_S2_V005.TBL 2,3
overlay [.TBL]SUM_AMW_BF_CELLREM_R1_S2_V006.TBL 2,3
overlay [.TBL]SUM_AMW_BF_CELLREM_R1_S2_V009.TBL 2,3
overlay [.TBL]SUM_AMW_BF_CELLREM_R1_S2_V010.TBL 2,3
overlay [.TBL]SUM_AMW_BF_CELLREM_R1_S2_V012.TBL 2,3
overlay [.TBL]SUM_AMW_BF_CELLREM_R1_S2_V014.TBL 2,3
overlay [.TBL]SUM_AMW_BF_CELLREM_R1_S2_V015.TBL 2,3
overlay [.TBL]SUM_AMW_BF_CELLREM_R1_S2_V016.TBL 2,3
overlay [.TBL]SUM_AMW_BF_CELLREM_R1_S2_V017.TBL 2,3
overlay [.TBL]SUM_AMW_BF_CELLREM_R1_S2_V018.TBL 2,3
overlay [.TBL]SUM_AMW_BF_CELLREM_R1_S2_V022.TBL 2,3
overlay [.TBL]SUM_AMW_BF_CELLREM_R1_S2_V023.TBL 2,3
overlay [.TBL]SUM_AMW_BF_CELLREM_R1_S2_V026.TBL 2,3
overlay [.TBL]SUM_AMW_BF_CELLREM_R1_S2_V027.TBL 2,3
overlay [.TBL]SUM_AMW_BF_CELLREM_R1_S2_V028.TBL 2,3
overlay [.TBL]SUM_AMW_BF_CELLREM_R1_S2_V029.TBL 2,3
overlay [.TBL]SUM_AMW_BF_CELLREM_R1_S2_V030.TBL 2,3
overlay [.TBL]SUM_AMW_BF_CELLREM_R1_S2_V034.TBL 2,3
overlay [.TBL]SUM_AMW_BF_CELLREM_R1_S2_V039.TBL 2,3
overlay [.TBL]SUM_AMW_BF_CELLREM_R1_S2_V040.TBL 2,3
overlay [.TBL]SUM_AMW_BF_CELLREM_R1_S2_V041.TBL 2,3
overlay [.TBL]SUM_AMW_BF_CELLREM_R1_S2_V042.TBL 2,3
overlay [.TBL]SUM_AMW_BF_CELLREM_R1_S2_V043.TBL 2,3
overlay [.TBL]SUM_AMW_BF_CELLREM_R1_S2_V045.TBL 2,3
overlay [.TBL]SUM_AMW_BF_CELLREM_R1_S2_V046.TBL 2,3
overlay [.TBL]SUM_AMW_BF_CELLREM_R1_S2_V047.TBL 2,3
overlay [.TBL]SUM_AMW_BF_CELLREM_R1_S2_V051.TBL 2,3
overlay [.TBL]SUM_AMW_BF_CELLREM_R1_S2_V052.TBL 2,3
overlay [.TBL]SUM_AMW_BF_CELLREM_R1_S2_V053.TBL 2,3
overlay [.TBL]SUM_AMW_BF_CELLREM_R1_S2_V064.TBL 2,3
overlay [.TBL]SUM_AMW_BF_CELLREM_R1_S2_V067.TBL 2,3
overlay [.TBL]SUM_AMW_BF_CELLREM_R1_S2_V068.TBL 2,3
overlay [.TBL]SUM_AMW_BF_CELLREM_R1_S2_V072.TBL 2,3
overlay [.TBL]SUM_AMW_BF_CELLREM_R1_S2_V073.TBL 2,3
overlay [.TBL]SUM_AMW_BF_CELLREM_R1_S2_V076.TBL 2,3
overlay [.TBL]SUM_AMW_BF_CELLREM_R1_S2_V077.TBL 2,3
overlay [.TBL]SUM_AMW_BF_CELLREM_R1_S2_V078.TBL 2,3
overlay [.TBL]SUM_AMW_BF_CELLREM_R1_S2_V079.TBL 2,3
overlay [.TBL]SUM_AMW_BF_CELLREM_R1_S2_V082.TBL 2,3
overlay [.TBL]SUM_AMW_BF_CELLREM_R1_S2_V085.TBL 2,3
overlay [.TBL]SUM_AMW_BF_CELLREM_R1_S2_V086.TBL 2,3
overlay [.TBL]SUM_AMW_BF_CELLREM_R1_S2_V087.TBL 2,3
overlay [.TBL]SUM_AMW_BF_CELLREM_R1_S2_V089.TBL 2,3
overlay [.TBL]SUM_AMW_BF_CELLREM_R1_S2_V090.TBL 2,3
overlay [.TBL]SUM_AMW_BF_CELLREM_R1_S2_V091.TBL 2,3
overlay [.TBL]SUM_AMW_BF_CELLREM_R1_S2_V093.TBL 2,3
overlay [.TBL]SUM_AMW_BF_CELLREM_R1_S2_V099.TBL 2,3
overlay [.TBL]SUM_AMW_BF_CELLREM_R1_S2_V100.TBL 2,3
replot 0,1E+4,0,1E+0,5,4,5,4
exit
```

Byle, Kathleen A

From: Chavez, Mario Joseph
Sent: Thursday, March 04, 2004 5:50 PM
To: Byle, Kathleen A
Subject: Signature Authority

Kathleen Byle 03-04-04

Kathleen,

Please sign the cover page for the following two documents for me tomorrow:

1. Effect of Naturally Occurring Sulfate on the MgO Safety Factor in the Presence of Supercompacted Waste and Heterogeneous Waste Emplacement, and

2. Effect of Waste Porosity Modeling on AMW Performance Assessment

All my comments are resolved and I have no outstanding issues.

Mario

Shoemaker, Paul E

From: Kessel, David S
Sent: Wednesday, March 03, 2004 5:41 PM
To: Shoemaker, Paul E
Cc: Chavez, Mario Joseph
Subject: Signature delegation for AMW reports

Paul E. Shoemaker
02/03/2004

Paul,
I have performed the management review for two AMW related reports and have no comments that are outstanding:

1. AMWTP Calculations: Effect of Waste Porosity Modeling on Performance Assessment (Cliff Hansen)
2. Effect of naturally Occurring Sulfate on the MgO Safety Factor in the Presence of Supercompacted Waste and Heterogeneous Waste Emplacement (Joe Kanney)

Please sign the cover pages of these reports for me.

Dave Kessel